Ore Geology Reviews 74 (2016) 63–75

Contents lists available at ScienceDirect

Ore Geology Reviews

journal homepage: www.elsevier.com/locate/oregeorev

Hydrothermal zircon geochronology: Age constraint on Nanling Range tungsten mineralization (Southeast China)

Xiang Wang [a,*], Jie Chen [a], Minghua Ren [b]

[a] School of Earth Sciences and Engineering, Nanjing University, 210046 Nanjing, PR China
[b] Department of Geoscience, University of Nevada, Las Vegas, Las Vegas, NV 89154-4010, USA

ARTICLE INFO

Article history:
Received 8 July 2015
Received in revised form 12 October 2015
Accepted 14 October 2015
Available online 10 November 2015

Keywords:
Hydrothermal zircon
U–Pb dating
Wolframite-bearing quartz veins
Biotite monzogranite
Nanling Range

ABSTRACT

The Nanling Range (Southeast China) is well known for its wolframite-bearing-quartz-vein (WQV) tungsten deposit. This study focuses on the geochemistry and geochronology of zircons from the WQV and challenges the current view of the tungsten mineralization in the Nanling Range. The features of the WQV zircons include: (1) pale brown, murky brown, or orange-red color and translucence under microscope; (2) {110} + {101} type crystal form; (3) weak cathodoluminescence; (4) enrichment of Hf (ranging from 1.97 to 7.83 wt.% HfO_2), U (ranging from 0.02 to 3.97 wt.% UO_2), Th (ranging from 0 to 0.65 wt.% ThO_2), and P (ranging from 0 to 1.82 wt.% P_2O_5); and (5) presence of solid (hydrothermal and ore minerals) and fluid inclusions. These features indicate that the WQV zircons crystallized from hydrothermal fluids during tungsten mineralization. The in-situ LA-ICPMS U–Pb results of the WQV zircons from five different tungsten deposits in the Nanling Range yield similar ages, ranging from 134.4 ± 1.9 Ma to 132.9 ± 1.5 Ma, approximately 20 million years younger than proposed tungsten ore ages (155 ± 5 Ma). Several mineralization characteristics and field observations also cast doubt on the current model — Nanling Range tungsten ore is the result of orthomagmatic processes. The zircon characterization method provided in this study could be applied to tungsten metallogenic research in other parts of the world.

1. Introduction

China has the richest tungsten resources in the world, with 6.55 million tons of total WO_3 proved reserve (Xu et al., 2008). Since 1996, more than 75% of world's tungsten production has come from China (Hua et al., 2010; Shedd, 2015). More than 90% of Chinese tungsten resources are stored in the Nanling Range (Southeast China), where dozens of giant and several hundred medium and small tungsten deposits exist (Hua et al., 2007; Mao et al., 2007).

Tungsten ore in the Nanling Range mainly occurs as wolframite-bearing quartz veins (WQV) (Fig. 1). WQV-type deposits account for 77% of all tungsten deposits in the Nanling Range (Xu et al., 2008). Previous studies associated this type of tungsten ore with early Yanshanian biotite monzogranite (BM) in the Nanling Range. This assumption is based on two lines of evidence: (1) Radiometric ages of most tungsten deposits fall around 155 ± 5 Ma (Chen et al., 2006b; Lu et al., 2006; Peng et al., 2007; Mao et al., 2007; Liu et al., 2008; Yuan et al., 2008; Wang et al., 2012b; Zeng et al., 2009; Zhang et al., 2009; Hua et al., 2010; Lei et al., 2010; Bai et al., 2013; and references therein), which is contemporary with the early Yanshanian BM (150–160 Ma) (Hua, 2005; Li et al., 2007a; Shen et al., 2007; Mao et al., 2007; Zhang et al., 2008; Yang et al., 2009; Li et al., 2011; Shu et al., 2011; Fang et al., 2012; and references therein), and (2) Tungsten deposits occur either adjacent to granitic plutons (Cai et al., 2006; Chen et al., 2006b; Xu et al., 2008; Guo et al., 2010), or within the plutons (Guo et al., 2010; Feng et al., 2011). Based on these observations, most researchers accept the metallogenic correlation between BM and WQV-type tungsten deposit (Mao et al., 2004; Mei et al., 2004; Shu et al., 2011; Xu et al., 2011; and references therein). An orthomagmatic model was proposed for the tungsten mineralization in the Nanling Range (Mao et al., 2007; Xi et al., 2007; Zhou et al., 2010), i.e., the ore formed from fractional crystallization of granitic magma (Burnham, 1979; Candela, 1997; Audétat, 2000; Pirajno, 2009). However, this model does not explain the source of the tungsten, the metal concentration mechanism, and the cross-cutting relationship between the WQV and the BM (detailed discussion in Section 6). The purpose of this paper is to clarify whether or not the tungsten mineralization was directly correlated with the early Yanshanian BM.

One key to answering whether the tungsten was derived from Jurassic BM magma is to better constrain when tungsten mineralization occurred. The ages of hydrothermal minerals or ore minerals associated with wolframite have been used as proxies for the origin of tungsten mineral system (Chen et al., 2006b; Lu et al., 2006; Peng et al., 2007; Yuan et al., 2008; Wang et al., 2012b; Zeng et al., 2009; Zhang et al., 2009; Hua et al., 2010; Lei et al., 2010; Bai et al., 2013). The ore ages

* Corresponding author at: 163 Xianlin Street, 210046, Nanjing, PR China.
E-mail address: xwang@nju.edu.cn (X. Wang).

http://dx.doi.org/10.1016/j.oregeorev.2015.10.034
0169-1368/

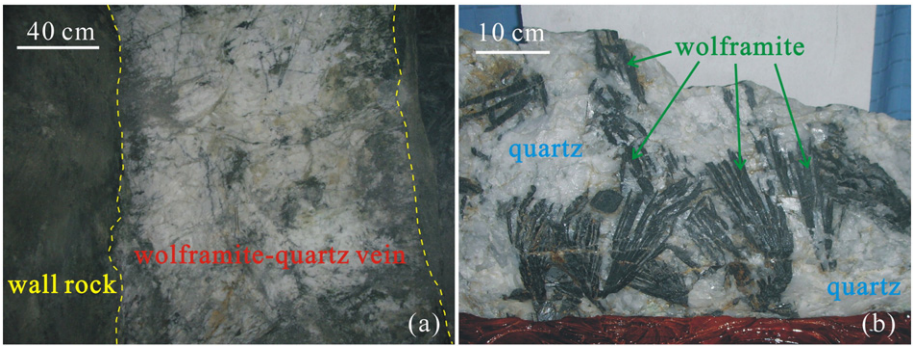

Fig. 1. Selected details of tungsten ore. (a) WQV from the Dajishan deposit; the WQV crosscuts the BM. Wolframite coexists with quartz or forms tiny veins along fractures. (b) Wolframite crystals in quartz vein from the Piaotang deposit.

(i.e., 155 ± 5 Ma), which are currently accepted, were measured by using the traditional geochronological methods (K–Ar, Ar–Ar, Rb–Sr, Sm–Nd, Re–Os, etc.). Unfortunately, these prevailing dating methods have some limitations, such as very low closure temperature, low contents of appropriate isotopes, or widely dispersed isotopic initial values. Some uncertainty is commonly induced by using these traditional geochronological methods (Dodson and McCleland-Brown, 1985; DePaolo, 1988; Dickin, 1995).

In this research, zircons separated from WQV samples have been studied. WQV zircons show similar characters as the zircons from granitic pegmatite (see Section 3). We use term "hydrothermal zircon here to indicate that these zircons were formed from high temperature fluids with high metal contents, which are physically and chemically similar to the fluids responsible for the genesis of granitic pegmatite. WQV zircons coexist with the ore mineral, wolframite and should form from the same hydrothermal fluids. Therefore, it is logical to take the WQV zircon U-Pb age as the crystallization time of WQV system. Our data show that these zircons have Early Cretaceous ages, significantly younger than the currently accepted age for WQV mineralization.

2. Analytical methods

Cathodoluminescence (CL) images were collected by using a JEOL JXA-8100 electron microprobe in the "State Key Laboratory for Mineral Deposits Research (SKLMDR), Nanjing University (China)". The operating conditions were 15 kV accelerating voltage and 20 nA beam current. Zircon chemistry was determined at the University of Texas at El Paso (UTEP) with a Cameca SX50 and University of Nevada, Las Vegas (UNLV) with a JEOL 8900 superprobe. Analyses were performed using 15 kV accelerating voltage, 50 nA beam current, 1 μm beam size, and 30 s peak counting time. Micro-Analysis Consultants Ltd. (MAC) standards were used for calibrating Si, Zr, and Hf contents in zircon, U in REE-U glass; Th in ThO_2; Y in YAG-garnet; and P, La, Ce, and Yb in synthetic REE phosphates. Zircon analyses are presented in Table 1.

In-situ U–Th–Pb isotopic compositions of zircons were determined using an Agilent 7500a ICP-MS coupled with a New Wave UP213 laser ablation system in the SKLMDR. Helium carrier gas was used to transport the ablated particles from the standard laser-ablation cell, which was then mixed with Ar gas via a mixing chamber before entering the ICP-MS torch. Laser beam had 18–25 μm diameter and used a repetition rate of 5 Hz. GJ-1 was used as an external standard with a recommended $^{206}Pb/^{207}Pb$ age of 608.5 ± 1.5 Ma (Jackson et al., 2004). Zircon standard Mud Tank (intercept age of 732 ± 5 Ma; Black and Gulson, 1978) was used to monitor analytical accuracy. U–Pb ages were calculated from the raw signal data using the on-line software package GLITTER (ver. 4.4) (Griffin et al., 2008). The calculations of weighted average ages and concordia plots were performed by using the ISOPLOT program (ver. 2.06) of Ludwig (1999). The ages are reported with 1σ errors.

3. Definition of hydrothermal zircon

The term hydrothermal zircon was introduced by Taubeneck (1957) and Davis et al. (1968). Since the 1980s, there has been a sharp increase in the study of hydrothermal zircon (Rubin et al., 1989, 1993; Claoué-Long et al., 1990; Kerrich and King, 1993; Uher and Černý, 1998; Grieco et al., 2001; Tomascheck et al., 2003; Hoskin, 2005; Schaltegger et al., 2005; Pelleter et al., 2007; Crowley et al., 2008). From the 1990s, hydrothermal zircon U–Pb geochronology has provided valuable information about metallogenesis (Claoué-Long et al., 1990; Kerrich and King, 1993; Dubinska et al., 2004; Crowley et al., 2008).

The origin of hydrothermal fluids can be complex and can include mantle-derived fluid (Grieco et al., 2001), granite-derived fluids (Rubin et al., 1989), or metamorphic fluids (Tomascheck et al., 2003). The crystallization mechanism of hydrothermal zircon can also differ, either directly crystallizing from a fluid (Hoskin, 2005) or recycled from metamict zircon (Pelleter et al., 2007). Hydrothermal zircon can show large variations in shape and composition (Claoué-Long et al., 1990; Fu et al., 2009). Evolved granitic magma is usually accompanied by enrichment of Zr (Erlank et al., 1978; Linnen and Keppler, 2002) as well as volatiles (including H_2O, F, Cl, B, P, S, and CO_2) (London, 1992; Webster and Rebbert, 1998). Along with the dropping of the magmatic pressure and/or temperature, incompatible trace elements and volatiles can differentiate from the residual magma (Audétat et al., 2008) and concentrate in the hydrothermal fluids within fractures. Hydrothermal zircon usually coexists with other hydrothermal minerals as well as ore minerals (Rubin et al., 1993; Hoskin, 2005).

There is no systematic way to easily distinguish hydrothermal zircon from the WQV. Determining distinctive features of hydrothermal zircon relative to magmatic and/or metamorphic zircon is one of the primary objectives of this study. Since hydrothermal fluid often is derived from highly differentiated granitic magma, the hydrothermal zircon is likely to inherit two important properties: (1) Crystallization temperature of hydrothermal zircon should be lower than that of magmatic zircon, and (2) Chemical composition of hydrothermal zircon should reflect that of hydrothermal fluid, which is commonly enriched in incompatible elements (Harris et al., 2004; Thomas et al., 2005). In some igneous systems, highly evolved granitic-pegmatitic melt may be comparable to high-temperature hydrothermal fluids. Thus, the characteristics of pegmatitic zircon can be used as guiding the study of hydrothermal zircon (Rubin et al., 1989; Partington et al., 1995; Uher and Černý, 1998; van Lichtervelde et al., 2007).

4. Distinguishing characteristics of hydrothermal zircon

Nine tungsten deposits in the Nanling Range (six in Jiangxi Province, two in Hunan Province, and one in Fujian Province) were studied (Fig. 2). Approximately 30 kg of wolframite-sulfide-mica-bearing quartz veins were collected from each deposit. These samples were

Table 1
Microprobe analyses (wt.%) of the hydrothermal zircons from the WQV in the Dangping (DP-3), Hukeng (HK-3), Tieshanlong (TSL-3), Taoxikeng (TXK-3) and Yaogangxian (YGX-6) tungsten deposits.

Sample	Grain	Point	HfO_2	UO_2	ThO_2	P_2O_5	Others[a]	ZrO_2	SiO_2	Total	Th/U
	1–01	#1	2.40	1.02	0.13	0.20	0.29	64.1	31.7	99.9	0.13
	1–02	#2	3.12	0.86	0.02	0.21	0.38	64.0	32.1	100.7	0.03
	1–04	#3	2.81	0.70	0.09	0.14	0.10	64.3	31.9	100.1	0.13
	1–05	#4	2.44	2.07	0.30	0.25	0.59	61.2	31.0	97.9	0.14
		#5	3.86	0.32	0.03	0.16	0.07	64.4	32.0	100.9	0.10
	1–07	#6	2.55	1.57	0.09	0.40	0.46	61.6	30.9	97.6	0.06
	1–11	#7	2.49	2.17	0.31	0.28	0.78	61.3	30.8	98.1	0.14
	1–12	#8	2.97	1.10	0.08	0.16	0.56	63.5	31.7	100.1	0.07
		#9	5.10	0.84	0.09	0.61	1.55	60.5	30.8	99.4	0.10
	1–13	#10	2.28	1.16	0.19	0.20	0.64	64.1	31.5	100.1	0.16
	1–14	#11	2.53	2.50	0.29	0.21	0.83	61.7	30.9	99.0	0.12
DP-3		#12	2.86	0.70	0.08	0.14	0.13	64.2	31.7	99.8	0.12
	1–15	#13	2.61	0.90	0.09	0.21	0.54	64.0	31.8	100.1	0.10
	1–17	#14	2.99	1.37	0.12	0.33	0.55	62.3	31.2	98.9	0.09
	1–18	#15	4.20	1.03	0.14	0.45	0.63	61.8	31.4	99.7	0.14
	1–19	#16	2.99	0.37	0.03	0.16	0.12	64.4	31.9	100.0	0.08
		#17	2.68	2.14	0.28	0.53	1.11	61.1	30.9	98.8	0.13
	1–20	#18	2.63	0.86	0.16	0.17	0.28	62.9	31.4	98.4	0.18
	1–21	#19	2.22	0.29	0.33	0.05	0.11	63.8	31.5	98.3	1.13
	1–28	#20	3.59	2.13	0.16	0.85	1.23	60.1	28.5	96.6	0.07
	1–31	#21	2.38	1.86	0.00	0.31	0.53	62.9	31.3	99.3	0.00
	1–34	#22	2.54	1.55	0.10	0.28	0.77	63.3	31.5	100.0	0.06
		#23	2.97	1.49	0.14	0.21	0.54	61.8	31.3	98.4	0.09
	2–02	#1	7.41	3.97	0.29	0.78	1.36	56.4	30.2	100.3	0.07
	2–03	#2	7.02	2.14	0.14	0.90	0.88	58.5	30.6	100.1	0.07
	2–04	#3	16.58	0.40	0.18	0.45	0.49	53.9	31.7	103.7	0.45
	2–07	#4	7.17	1.79	0.27	0.52	1.95	55.0	29.2	95.9	0.15
	2–08	#5	3.56	0.09	0.11	0.31	0.29	62.3	30.8	97.4	1.29
	2–10	#6	7.35	0.66	0.11	0.53	0.52	60.3	31.2	100.6	0.16
	2–17	#7	7.83	0.91	0.18	0.44	1.08	58.8	30.8	100.0	0.20
	2–24	#8	5.10	1.62	0.12	1.14	0.62	58.9	30.1	97.6	0.07
	2–25	#9	5.07	0.85	0.15	1.02	0.41	59.8	30.1	97.5	0.18
HK-3	2–26	#10	2.58	0.09	0.08	0.03	0.20	65.6	32.1	100.7	0.91
	1–04	#1	6.21	1.82	0.00	0.66	0.33	58.0	30.3	97.3	0.00
	1–08	#2	5.24	1.59	0.00	0.53	0.17	60.2	31.1	98.8	0.00
	1–20	#3	3.91	1.42	0.00	0.30	0.12	61.8	31.7	99.3	0.00
	1–22	#4	5.00	1.34	0.06	0.42	0.18	60.2	30.8	98.0	0.04
	1–26	#5	2.10	1.11	0.07	0.05	0.15	63.0	31.6	98.2	0.06
	2–10	#6	2.34	0.91	0.00	0.12	0.08	63.4	31.8	98.6	0.00
		#7	3.09	1.70	0.00	0.45	0.31	60.6	30.7	96.9	0.00
TLS-3	2–20	#8	2.71	0.35	0.00	0.00	0.06	63.9	31.8	98.8	0.00
	2–23	#9	3.42	2.88	0.01	0.92	0.61	57.8	29.6	95.3	0.00
		#10	3.18	0.84	0.00	0.15	0.00	62.8	31.3	98.2	0.00
	2–25	#11	2.48	0.95	0.00	0.12	0.03	63.4	31.9	98.9	0.00
	2–28	#12	7.42	2.78	0.09	1.20	1.45	53.3	28.8	95.0	0.03
	2–35	#13	5.13	0.92	0.18	0.31	0.34	60.1	30.1	97.1	0.20
	2–39	#14	5.37	2.10	0.21	1.08	0.57	57.4	30.1	96.8	0.10
	2–44	#15	2.67	1.93	0.10	0.50	0.47	58.8	29.7	94.2	0.05
		#1	3.38	0.89	0.07	0.46	0.53	62.4	30.9	98.7	0.08
		#2	5.11	0.32	0.00	0.37	0.14	62.9	31.5	100.4	0.00
	1–05	#3	5.36	0.30	0.08	0.18	0.10	62.0	31.7	99.8	0.28
	2–01	#4	2.62	0.58	0.24	0.14	0.21	64.5	31.8	100.1	0.42
	2–03	#5	3.13	0.61	0.06	0.29	0.06	63.2	31.4	98.7	0.10
		#6	2.88	0.78	0.06	0.24	0.08	64.4	32.1	100.6	0.08
	2–05	#7	1.97	1.00	0.31	0.47	0.29	61.5	30.3	95.8	0.31
	2–06	#8	2.88	1.09	0.08	0.42	0.15	61.8	30.3	96.7	0.07
		#9	2.99	0.96	0.00	0.38	0.20	62.6	31.7	98.8	0.00
		#10	2.58	0.69	0.25	0.36	0.29	62.1	30.7	97.0	0.36
		#11	2.66	0.48	0.09	0.35	0.34	65.3	32.3	101.5	0.18
	2–07	#12	2.87	1.07	0.10	0.69	0.17	62.2	30.6	97.8	0.09
		#13	3.46	1.23	0.02	0.47	0.11	62.9	31.5	99.7	0.02
		#14	2.97	1.31	0.12	0.54	0.11	63.0	31.6	99.7	0.09
	2–08	#15	2.27	0.68	0.09	0.15	0.03	64.4	31.7	99.3	0.13
	2–13	#16	2.47	0.71	0.14	0.17	0.09	64.1	31.7	99.4	0.20
	2–20	#17	3.24	1.31	0.24	0.56	1.12	60.7	30.3	97.5	0.18
	2–23	#18	2.38	0.34	0.07	0.05	0.14	64.7	31.9	99.6	0.22
	2–24	#19	2.81	0.71	0.06	0.34	0.16	64.0	31.9	99.9	0.09
	2–26	#20	2.43	0.40	0.13	0.18	0.22	64.3	31.3	99.0	0.33
	2–34	#21	3.00	1.11	0.16	0.51	0.61	59.9	29.8	95.1	0.14
		#22	2.93	0.99	0.07	0.49	0.11	63.3	31.4	99.3	0.07
	2–36	#23	6.62	0.36	0.13	0.12	0.06	60.9	31.2	99.4	0.35
	2–38	#24	3.04	1.64	0.12	0.72	0.45	60.8	30.2	97.0	0.07
TXK-3		#25	3.02	2.07	0.24	0.73	0.51	60.3	30.1	97.0	0.12

(continued on next page)

Table 1 (*continued*)

Sample	Grain	Point	HfO_2	UO_2	ThO_2	P_2O_5	Others[a]	ZrO_2	SiO_2	Total	Th/U
		#26	2.90	1.81	0.13	0.84	0.68	60.1	29.9	96.3	0.07
	2–40	#27	2.53	1.31	0.31	0.38	0.03	61.7	30.4	96.7	0.24
	2–50	#28	2.29	0.86	0.00	0.58	0.19	62.8	31.8	98.5	0.00
		#29	2.22	0.76	0.00	0.42	0.22	64.3	32.1	100.0	0.00
		#1	2.08	2.47	0.65	1.09	3.07	53.2	25.9	88.5	0.26
	1–10	#2	2.83	1.04	0.07	0.00	0.07	62.7	31.0	97.7	0.07
	1–21	#3	2.72	0.02	0.00	0.00	0.05	64.9	31.6	99.3	0.00
		#4	2.35	2.77	0.22	1.54	5.29	44.4	24.5	81.1	0.08
	1–25	#5	2.08	3.96	0.48	1.82	3.50	48.7	25.1	85.7	0.12
	2–02	#6	4.90	2.60	0.15	0.79	1.78	54.1	28.2	92.5	0.22
	2–03	#7	3.18	1.49	0.04	0.14	0.10	60.3	30.1	95.3	0.26
		#8	2.40	1.11	0.17	0.00	0.10	62.7	31.1	97.6	0.00
	2–05	#9	2.11	7.04	0.72	0.56	1.70	52.9	27.7	92.7	1.00
	2–06	#10	2.51	0.27	0.06	0.00	0.12	63.5	31.1	97.5	0.02
	2–07	#11	2.30	0.50	0.13	0.00	0.04	62.9	31.1	97.0	0.00
	2–13	#12	5.12	0.43	0.00	0.00	0.05	61.8	31.4	98.8	0.00
	2–19	#13	3.77	0.23	0.23	0.02	0.57	53.6	27.4	85.8	0.00
		#14	2.91	1.14	0.02	0.00	0.10	62.3	31.3	97.8	0.00
		#15	3.59	0.73	0.00	0.30	0.28	60.2	30.1	95.2	0.13
	2–21	#16	4.43	0.68	0.00	0.04	0.08	62.4	31.4	99.1	0.00
		#17	3.97	0.65	0.00	0.00	0.11	62.3	30.5	97.6	0.40
YGX-6	2–33	#18	3.79	0.44	0.00	0.00	0.02	61.6	30.8	96.6	0.19

[a] Others mainly include contents of Y_2O_3, Ce_2O_3, Al_2O_3, La_2O_3, and MnO.

processed through the standard mineral separation techniques, including crushing, pulverizing, concentrating accessory mineral by heavy liquid and magnetic separator. Sulfide was dissolved using dilute HNO_3 solution. Zircons were found in five samples from the nine deposits. All zircon grains were hand-picked under the binocular microscope, embedded in epoxy, and polished to expose their cores. The crystal shape, internal structure, and trace element content of the zircons have been studied. WQV zircons differ from magmatic zircons in granitic rocks, but are almost identical to hydrothermal zircons in granitic pegmatite and ore veins. Their characteristics are summarized below.

4.1. Color

All WQV zircons are more or less metamict. They are translucent and are pale brown, murky brown, or orange-red (Fig. 3). When zircon is

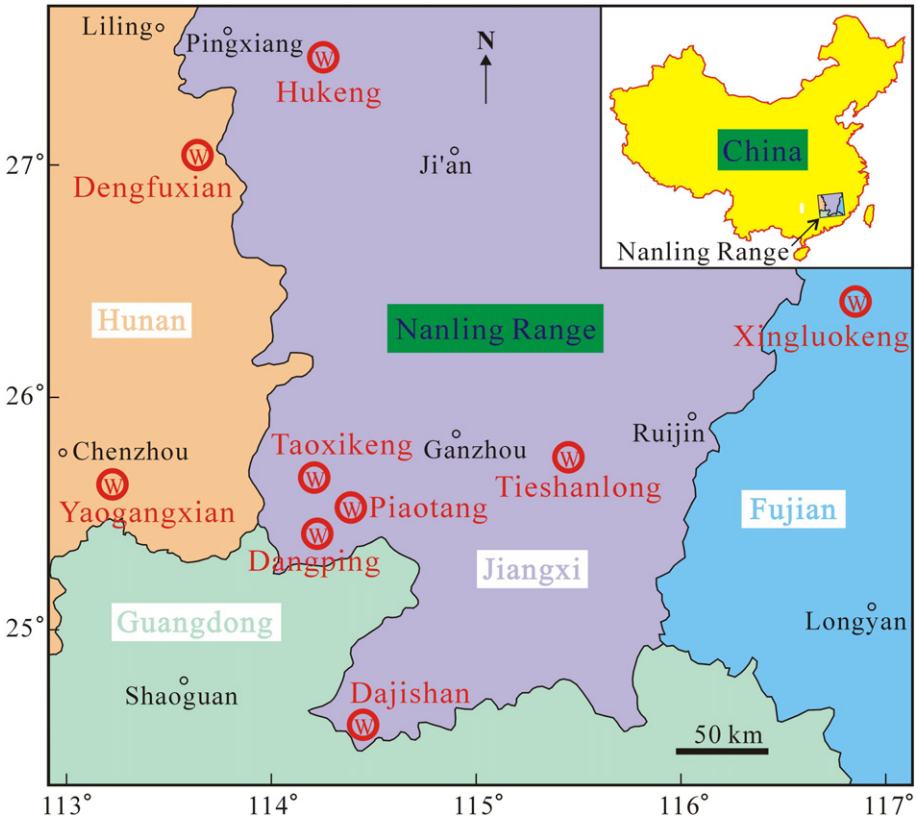

Fig. 2. Studied giant tungsten deposits (W) in the Nanling Range (South China): Hukeng, Tieshanlong, Taoxikeng, Piaotang, Dangping and Dajishan in Jiangxi Province, Dengfuxian and Yaogangxian in Hunan Province, and Xingluokeng in Fujian Province.

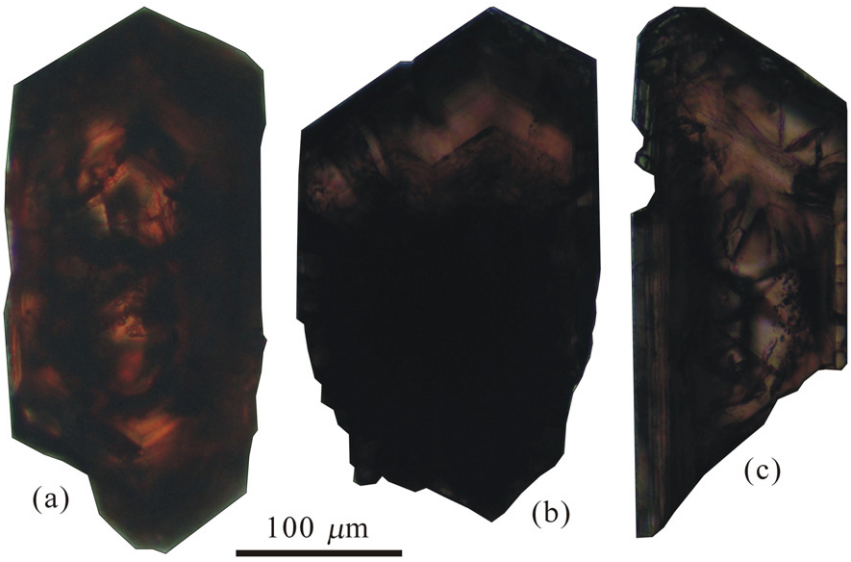

Fig. 3. Photomicrographs (transmitted light) of the hydrothermal zircons from WQV in the following tungsten deposits: (a) Yaogangxian, (b) Taoxikeng, and (c) Tieshanlong.

enriched in U and Th, the radiation of alpha particle from U and Th can cause lattice damage (i.e., metamictization). The subsequent microfissures in zircon can be filled by impurities (Ewing et al., 2003). The metamict zircons usually become translucent and colored, such as pegmatitic zircon (Černý and Slivola, 1980; Lumpkin, 1998). Hydrothermal zircons from Au-bearing quartz vein (Claoué-Long et al., 1990) and from altered rock (Dubinska et al., 2004) always have certain colors.

4.2. Morphology

WQV zircons almost exclusively have the {110} + {101} type crystallographic form with rare {211} pyramidal faces (Fig. 3). This characteristic is very similar to the typology of hydrothermal zircon from granitic pegmatite. The morphology of magmatic zircons from granitic rocks is commonly characterized by combination of {110} + {100} prismatic faces and {101} + {211} pyramidal faces. However, it shows a typological change toward simple combination of {110} prismatic faces and {101} pyramidal faces during the fractional crystallization of granitic magma (Pupin, 1980; Caironi et al., 2000; Wang et al., 2007), likely due to increasing fluid by fractional crystallization. Pegmatitic zircon generally shows the {110} + {101} type crystallographic form, occasionally with few {100} prismatic faces and/or {211} pyramidal faces (Uher and Černý, 1998; Crowley et al., 2008). Other studies show that the hydrothermal zircons in albitized rhyolitic tuff (Pelleter et al., 2007) and aplite (Hoskin, 2005) also have {110} + {101} type crystal form.

4.3. Internal structure

WQV zircons always show weak cathodoluminescence (CL) signal (Fig. 4). They usually contain relict cores with corroded outlines (Fig. 4a and b). Zircons usually contain rare earth elements, especially Dy and Tb, which are responsible for the CL (Blanc et al., 1994). Zircons commonly show oscillatory zoning and/or sector zoning structures (Claiborne et al., 2006). Recent research shows that CL brightness is highly affected by the crystallinity of zircon (Nasdala et al., 2003). Pegmatitic zircons, generally metamict due to high U and Th contents (Černý and Slivola, 1980; Lumpkin, 1998), commonly have extremely weak CL (Hoskin, 2005; Schaltegger et al., 2005; Crowley et al., 2008). Hydrothermal zircons with weak CL have been reported in the granitic aplite (Hoskin, 2005), granitic pegmatite (Rubin et al., 1989; Crowley et al., 2008), hydrothermally altered rock (Schaltegger et al., 2005), and ore-bearing quartz veins (Rubin et al., 1993; Hoskin, 2005).

4.4. Zircon chemistry

The WQV zircons differ in chemistry from magmatic zircons in granitic rocks, but are similar to the zircons from granitic pegmatites. All zircon analyses were performed on the rim area (dark in CL).

4.4.1. Hafnium

The WQV zircons have 1.97 to 7.83 wt.% HfO_2 (with one exceptionally high content of 16.58 wt.% HfO_2, Table 1), with a mode of 3.00 wt.% and a median of 2.93 wt.% (Fig. 5a). This is much higher than the HfO_2 of magmatic zircons from granitic rocks (with a mode of 1.43 wt.% and a median of 1.48 wt.%, Wang et al., 2010). This high Hf characteristic is similar to hydrothermal zircons from the Abitibi

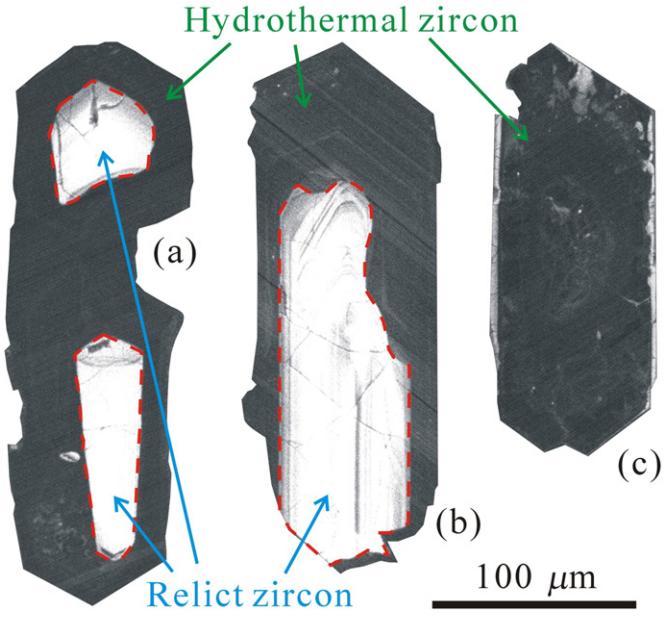

Fig. 4. CL image of WQV zircons from the following tungsten deposits: (a) Hukeng, (b) Dangping, (c) Taoxikeng. (a)–(b) The hydrothermal zircon contains relict core with eroded rim (marked by red dashed line); (c) The hydrothermal zircon is without relic core.

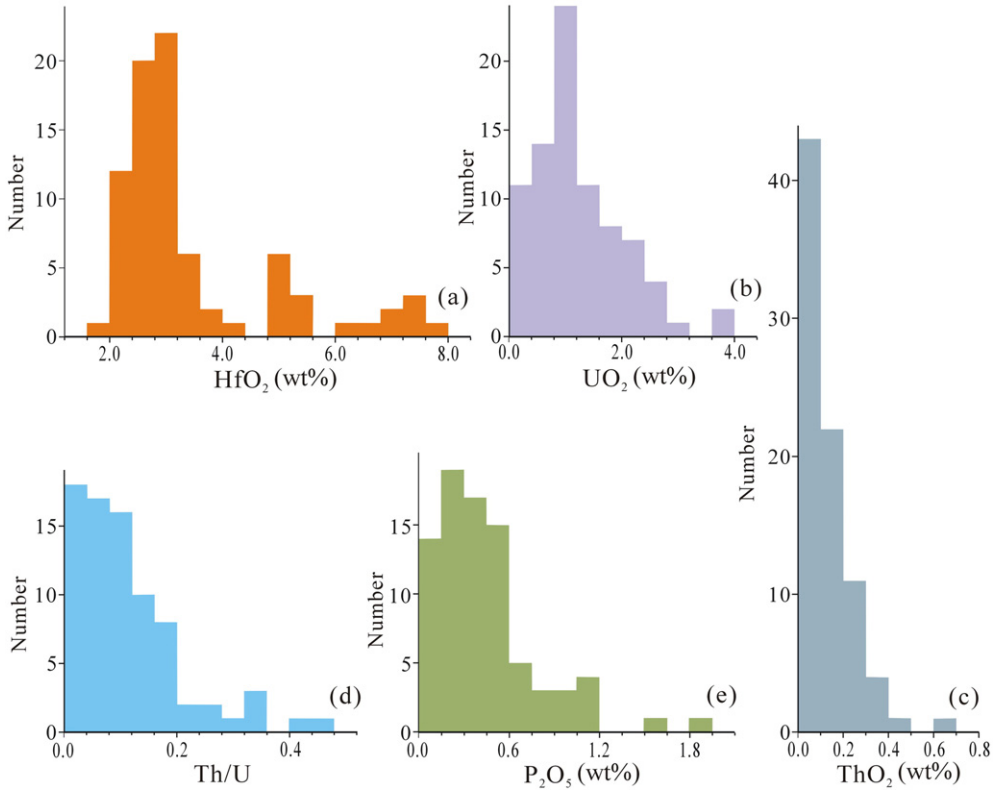

Fig. 5. Histograms of the minor elements in WQV zircons (data from Table 1): (a) HfO_2 (wt.%), (b) UO_2 (wt.%), (c) ThO_2 (wt.%), (d) Th/U ratios, (e) P_2O_5 (wt.%).

gold deposit quartz vein (Canada) and from veinlets in the F-rich Sierra Blanca intrusion (Texas, USA), which have HfO_2 up to 4.2 wt.% (Kerrich and King, 1993) and 7.6 wt.% (Rubin et al., 1993), respectively.

Even though Hf easily substitutes for Zr in zircon due to similar ionic radius (0.84 Å for Zr^{4+} and 0.83 Å for Hf^{4+} in octahedral coordination, Shannon, 1976), HfO_2 contents in magmatic zircons are generally less than 2 wt.% (Wang et al., 2010). Pegmatitic zircon can contain up to 35.2 wt.% HfO_2 (Zhang et al., 2004) due to Hf enrichment in hydrothermal fluid (Linnen and Keppler, 2002; Badanina et al., 2006). The mineral hafnon is identified in granitic pegmatites (Correia Neves and Nunes, 1974).

4.4.2. Uranium

WQV zircons contain 0.02 to 3.97 wt.% UO_2, with a mode of 1 wt.% and a median of 1.03 wt.% (Fig. 5b). In contrast, magmatic zircons from granitic rocks have much lower UO_2 contents with a mode of 0.0142 wt.% and a median of 0.0397 wt.% (Wang et al., 2011). WQV zircons are similar to hydrothermal zircons from granitic pegmatites, which have a median of 0.81 wt.% UO_2 (Gbelsky, 1979; Cassedanne et al., 1985; Wang et al., 1990; Zhang et al., 2004).

High U in highly fractionated granite-pegmatite (such as 400 ppm U in the Rössing granitic pegmatite, Namibia, Cuney, 1980) causes high U in hydrothermal zircons, ranging from 7.63 to 9.5 wt.% UO_2 (Gbelsky, 1979; Cassedanne et al., 1985; Wang et al., 1990). However, unlike Hf contents in hydrothermal zircons, U decreases from core to rim (Cassedanne et al., 1985; Wang et al., 1990; Zhang et al., 2004). This is because the somewhat large ionic radius (1.00 Å for U^{4+} in octahedral coordination, Shannon, 1976) prevents U entering zircon. Rather than entering zircon lattice, fluids with elevated uranium contents will form uraninite/uranmicrolite in the granitic pegmatite (Černý and Slivola, 1980; Cuney, 1980). Low temperature hydrothermal zircon (formed at 260–350 °C in quartz veins) contains 0.0022 to 0.0798 wt.% UO_2 (obtained by Sensitive High Resolution Ion Microprobe (SHRIMP); Claoué-Long et al., 1990).

4.4.3. Thorium

Pegmatitic zircons can contain 4.1 to 4.5 wt.% ThO_2 and coexist with thorite (Černý and Slivola, 1980; Cassedanne et al., 1985; Seidler et al., 2005). Since the ionic radius of Th is larger than that of U (1.05 Å for Th^{4+} in octahedral coordination, Shannon, 1976), the Th is in less favor of the zircon lattice. Thus Th/U ratios for most pegmatite zircons are low (Cassedanne et al., 1985; Partington et al., 1995).

WQV zircons have 0 to 0.65 wt.% ThO_2, with a mean of 0.13 wt.% and a median of 0.10 wt.% (Fig. 5c). In contrast, magmatic zircons from granitic rocks have a mean of 0.0337 wt.% and a median of 0.0159 wt.% ThO_2 (Wang et al., 2011). Th/U ratios of WQV zircons range from 0 to 0.45 (three outliers with Th/U 0.91, 1.13 and 1.29), with a mean of 0.15 and a median of 0.09 (Fig. 5d). This is somewhat lower than Th/U ratios of magmatic zircons from granitic rocks with a mean of 0.59 and a median of 0.52 (Wang et al., 2011). The high ThO_2 contents in the WQV zircons suggest that the hydrothermal fluid originated from highly differentiated granitic magma, and the low Th/U ratios of the WQV zircons indicates a low crystallization temperature.

4.4.4. Phosphorus

WQV zircons have 0 to 1.82 wt.% P_2O_5, with a mean of 0.43 wt.% and a median of 0.37 wt.% (Fig. 5e). Magmatic zircons from granitic rocks have a mean of 0.05 wt.% and a median of 0.04 wt.% P_2O_5 (Caironi et al., 2000; Wang et al., 2002, 2003). Enrichment of P in WQV hydrothermal fluids can be reflected by the crystallization of apatite, xenotime and monazite. Phosphate inclusions exist in WQV zircons (see Section 4.5).

As noted above, there are abundant substitutions in hydrothermal zircon, especially Hf, U, Th, etc. for Zr in octahedron sites and P, Al, V, etc. for Si in tetrahedral sites (Hoskin, 2005). Zircons from granitic pegmatites contain up to 2.6 wt.% P_2O_5 (Lumpkin, 1998; van Lichtervelde et al., 2007). This is probably related to the high P contents in the fluids that form granitic pegmatites, which usually contain apatite, xenotime, monazite, and some phosphate minerals (Masau et al., 2002;

Hetherington et al., 2008). Hoskin (2005) reported high P contents (~0.8 to 4 wt.%) in the hydrothermal zircon from the Boggy Plain pluton (eastern Australia).

4.5. Inclusions

WQV zircons contain inclusions in the form of (1) hydrothermal minerals such as quartz (Fig. 6f) and monazite (Fig. 6c), (2) ore minerals such as pyrite (Fig. 6d), thorite (Fig. 6a), and xenotime (Fig. 6b, e), and (3) gas–liquid inclusions (Fig. 6d).

The magmatic zircons from granitic rocks commonly contain inclusions of rock-forming minerals such as plagioclase, orthoclase, quartz, etc. (Minor and Mukasa, 1997; Nasdala et al., 1999; Pelleter et al., 2007), accessory minerals such as apatite, monazite, Fe–Ti oxide minerals, etc. (Minor and Mukasa, 1997; Nasdala et al., 1999), and magmatic melts (Thomas et al., 2003). On the other hand, zircons from granitic pegmatite and ore-bearing quartz veins mainly contain hydrothermal minerals such as fluorite, tourmaline, mica, monazite, calcite, topaz, alkali feldspar, quartz, etc. (Hoskin, 2005; Pelleter et al., 2007); ore minerals such as pyrite, xenotime, scheelite, thorite, coffinite or uraninite, thorite, cassiterite, galena, molybdenite, chalcopyrite, sphalerite, beryl, sphene, rutile, xenotime, arsenopyrite, etc. (Pelleter et al., 2007; van Lichtervelde et al., 2007); and primary fluid inclusions (Schaltegger et al., 2005). Thus, the presence of solid (hydrothermal and ore minerals) and fluid inclusions in WQV zircons indicates a hydrothermal environment of formation (Schaltegger et al., 2005; Pelleter et al., 2007).

5. Geochronology of the WQV zircons

WQV zircons contain adequate U and Th with little common Pb and is also mechanically and chemically inert (Heaman and Parrish, 1991). With the development of in-situ micro-analytical techniques, such as secondary ion mass spectrometry (SIMS) and laser ablation inductively coupled plasma mass spectrometry (LA-ICPMS), zircon geochronology can reveal the complex geologic history preserved within individual zircon grains (Ireland and Williams, 2003). However, zircon geochronology has not been applied extensively to vein-type metal deposits. The main reasons are: (1) rarity of hydrothermal zircon in ore-bearing quartz veins (Lu et al., 1999), and (2) Pb loss due to metamictization (Mezger and Krogstad, 1997). In spite of these problems, gold mineralization history has been successfully studied by U–Pb dating of the hydrothermal zircon from quartz veins since the 1990s (Claoué-Long et al., 1990; Kerrich and King, 1993).

No hydrothermal zircon U–Pb ages have been reported in vein-type tungsten deposits so far. This study is the first attempt to use hydrothermal zircon geochronology for constraining the age of tungsten mineralization. The following rules are keys to overcoming barriers in hydrothermal zircon dating: (1) During field sampling, it is important to collect quartz veins enriched in ore minerals (wolframite, cassiterite, pyrite, chalcopyrite, and molybdenite, etc.). Such samples usually contain hydrothermal zircon. (2) During LA-ICPMS zircon spot selection, it is critical to select the least metamict hydrothermal zircons. This type of zircon generally shows less discordant U–Pb ages. In this study, WQV zircon U–Pb isotopes from five tungsten deposits have

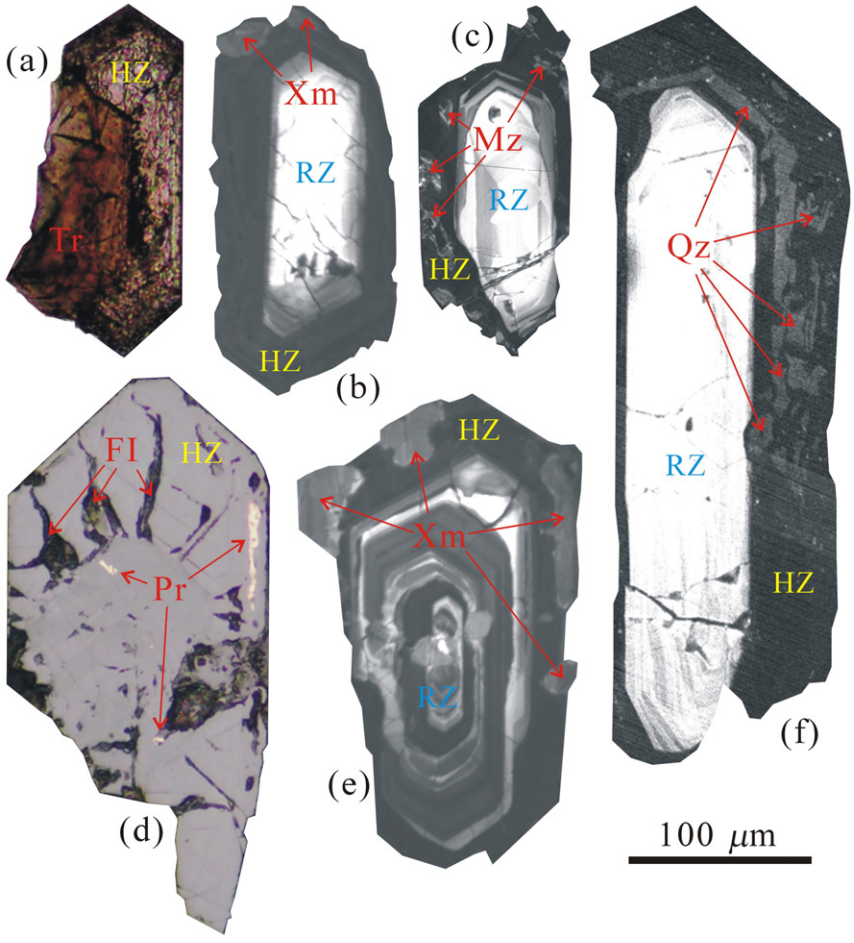

Fig. 6. Inclusions and relict zircon (RZ) within hydrothermal zircon (HZ): (a) transmitted light image showing thorite (Tr) associated with HZ from the Dangping deposit; (b) CL image showing xenotimes (Xm) within HZ from the Tieshanlong deposit; (c) CL image showing monazites (Mz) within HZ from the Hukeng deposit; (d) reflected light image showing pyrites (Pr) and fluid inclusions (Fl) within HZ from the Tieshanlong deposit; (e) CL image showing xenotimes (Xm) within HZ from the Tieshanlong deposit; (f) CL image showing quartz (Qz) within HZ from the Yaogangxian deposit.

Table 2
LA-ICPMS hydrothermal zircon U-Pb data from the WQV in the Dangping (DP-3), Hukeng (HK-3), Tieshanlong (TSL-3), Taoxikeng (TXK-3) and Yaogangxian (YGX-6) tungsten deposits, and from a mineralized greisen in the Xingluokeng (XLK-3) tungsten deposit.

Sample	Grain-Spot	Isotopic ratios						Apparent ages (Ma)					
		$^{206}Pb/^{238}U$	±1σ	$^{207}Pb/^{235}U$	±1σ	$^{207}Pb/^{206}Pb$	±1σ	$^{206}Pb/^{238}U$	±1σ	$^{207}Pb/^{235}U$	±1σ	$^{207}Pb/^{206}Pb$	±1σ
	104–1	0.02136	0.00028	0.14645	0.00270	0.04973	0.00088	136.2	1.8	138.8	2.4	182.3	40.7
	104–2	0.02111	0.00027	0.14553	0.00237	0.05002	0.00077	134.6	1.7	138.0	2.1	195.7	35.4
	104–3	0.02071	0.00030	0.13994	0.00344	0.04902	0.00120	132.1	1.9	133.0	3.1	148.7	56.6
	104–5	0.02083	0.00029	0.15535	0.00414	0.05412	0.00149	132.9	1.8	146.6	3.6	375.9	60.7
	106–1	0.02120	0.00028	0.15691	0.00273	0.05367	0.00087	135.3	1.8	148.0	2.4	357.3	36.1
	111–2	0.02077	0.00032	0.15827	0.00484	0.05527	0.00174	132.5	2.0	149.2	4.2	423.0	68.2
	112–2	0.02043	0.00028	0.14325	0.00251	0.05084	0.00080	130.4	1.8	135.9	2.2	233.7	35.8
	112–3	0.02100	0.00026	0.14442	0.00212	0.04989	0.00067	134.0	1.7	137.0	1.9	189.7	30.7
	113–1	0.02088	0.00025	0.14185	0.00209	0.04927	0.00068	133.2	1.6	134.7	1.9	160.9	31.9
	115–1	0.02102	0.00028	0.14307	0.00235	0.04937	0.00074	134.1	1.8	135.8	2.1	165.6	34.4
	117–2	0.02055	0.00028	0.14673	0.00392	0.05181	0.00144	131.1	1.8	139.0	3.5	277.1	62.3
	121–1	0.02131	0.00036	0.14526	0.00592	0.04946	0.00208	135.9	2.3	137.7	5.3	169.8	95.4
	132–2	0.02107	0.00029	0.14165	0.00399	0.04882	0.00143	134.4	1.8	134.5	3.6	139.4	67.6
DP-3	134–1	0.02097	0.00031	0.14103	0.00297	0.04876	0.00095	133.8	2.0	134.0	2.6	136.2	44.9
	205–2	0.02069	0.00039	0.14603	0.00650	0.05120	0.00238	132.0	2.5	138.4	5.8	249.6	103.6
	206–1	0.02099	0.00044	0.14605	0.00718	0.05054	0.00269	133.9	2.8	138.4	6.4	219.9	118.9
	208–1	0.02085	0.00029	0.14523	0.00284	0.05051	0.00093	133.0	1.8	137.7	2.5	218.7	41.9
	209–1	0.02076	0.00033	0.13943	0.00369	0.04872	0.00127	132.4	2.1	132.5	3.3	134.3	60.1
	210–2	0.02091	0.00034	0.14821	0.00455	0.05143	0.00159	133.4	2.1	140.3	4.0	260.1	69.7
	211–1	0.02089	0.00032	0.14977	0.00371	0.05196	0.00126	133.3	2.0	141.7	3.3	283.7	54.6
	218–2	0.02048	0.00040	0.15313	0.00683	0.05411	0.00251	130.7	2.6	144.7	6.0	375.3	100.7
HK-3	220–1	0.02101	0.00031	0.14298	0.00375	0.04935	0.00130	134.1	2.0	135.7	3.3	164.3	60.6
	104–1	0.02088	0.00036	0.19414	0.00759	0.06737	0.00277	133.2	2.3	180.2	6.5	849.3	83.3
	108–1	0.02136	0.00029	0.16829	0.00239	0.05711	0.00082	136.3	1.8	157.9	2.1	495.0	31.6
	120–1	0.02133	0.00027	0.19226	0.00260	0.06535	0.00090	136.0	1.7	178.6	2.2	785.8	28.7
	122–1	0.02129	0.00035	0.20738	0.00716	0.07063	0.00256	135.8	2.2	191.4	6.0	946.6	72.6
	122–2	0.02102	0.00042	0.23404	0.00870	0.08076	0.00318	134.1	2.6	213.5	7.2	1215.6	75.5
	128–2	0.02097	0.00029	0.15990	0.00385	0.05537	0.00146	133.8	1.8	150.6	3.4	427.1	57.2
	210–1	0.02166	0.00046	0.38096	0.01743	0.12802	0.00676	138.2	2.9	327.7	12.8	2071.0	90.2
	210–2	0.02105	0.00031	0.18980	0.00657	0.06597	0.00261	134.3	2.0	176.5	5.6	805.3	80.7
	212–1	0.02130	0.00044	0.16751	0.00934	0.05724	0.00422	135.8	2.8	157.3	8.1	500.4	155.0
	212–2	0.02167	0.00038	0.35565	0.01342	0.11942	0.00500	138.2	2.4	309.0	10.1	1947.6	73.0
	239–1	0.02077	0.00058	0.14835	0.00951	0.05204	0.00373	132.5	3.7	140.5	8.4	287.3	155.5
	239–2	0.02127	0.00066	0.26348	0.01905	0.08958	0.00704	135.7	4.2	237.5	15.3	1416.6	143.3
	239–3	0.02120	0.00034	0.30176	0.01441	0.10786	0.00683	135.2	2.2	267.8	11.2	1763.6	111.4
	244–2	0.02104	0.00037	0.15833	0.00728	0.05545	0.00309	134.2	2.3	149.2	6.4	430.3	120.0
	244–3	0.02084	0.00047	0.14154	0.00802	0.04940	0.00318	133.0	2.9	134.4	7.1	167.1	143.7
TSL-3	244–5	0.02114	0.00047	0.15218	0.00931	0.05267	0.00370	134.9	3.0	143.8	8.2	314.8	151.6
	101–1	0.02133	0.00033	0.15189	0.00349	0.05164	0.00119	136.1	2.1	143.6	3.1	269.6	52.2
	105–1	0.02112	0.00025	0.15440	0.00219	0.05304	0.00077	134.7	1.6	145.8	1.9	330.5	32.3
	105–2	0.02090	0.00030	0.14275	0.00325	0.04955	0.00114	133.4	1.9	135.5	2.9	174.0	52.6
	105–3	0.02117	0.00030	0.14221	0.00297	0.04868	0.00101	135.1	1.9	135.0	2.6	132.4	48.3
	201–1	0.02124	0.00026	0.16770	0.00166	0.05725	0.00056	135.5	1.6	157.4	1.5	500.8	21.6
	207–1	0.02122	0.00026	0.16093	0.00172	0.05501	0.00058	135.3	1.7	151.5	1.5	412.7	23.0
	211–1	0.02105	0.00032	0.14159	0.00235	0.04878	0.00080	134.3	2.0	134.5	2.1	137.5	38.0
	213–2	0.02111	0.00033	0.14475	0.00380	0.04978	0.00128	134.7	2.1	137.3	3.4	184.9	58.9
TXK-3	213–4	0.02130	0.00024	0.16940	0.00227	0.05768	0.00081	135.9	1.5	158.9	2.0	517.5	31.0
	110–1	0.02080	0.00038	0.14621	0.00515	0.05102	0.00183	132.7	2.4	138.6	4.6	241.5	80.4
	114–2	0.02107	0.00036	0.14217	0.00399	0.04895	0.00132	134.4	2.3	135.0	3.6	145.5	62.1
	114–3	0.02107	0.00040	0.14178	0.00541	0.04881	0.00188	134.4	2.5	134.6	4.8	138.5	88.2
	120–1	0.02119	0.00045	0.14331	0.00692	0.04906	0.00243	135.2	2.8	136.0	6.2	150.7	112.0
	202–3	0.02118	0.00028	0.14235	0.00318	0.04875	0.00110	135.1	1.8	135.1	2.8	135.7	52.0
	202–4	0.02087	0.00028	0.14289	0.00359	0.04968	0.00127	133.2	1.8	135.6	3.2	179.8	58.6
	203–3	0.02085	0.00026	0.14525	0.00319	0.05054	0.00114	133.0	1.7	137.7	2.8	219.9	51.2
	203–4	0.02117	0.00041	0.14615	0.00691	0.05011	0.00247	135.1	2.6	138.5	6.1	200.2	110.4
	208–1	0.02053	0.00037	0.14406	0.00570	0.05086	0.00204	131.0	2.3	136.7	5.1	234.6	90.1
	215–1	0.02072	0.00049	0.14352	0.00848	0.05026	0.00305	132.2	3.1	136.2	7.5	207.1	135.0
	222–2	0.02103	0.00032	0.14492	0.00322	0.04999	0.00104	134.2	2.0	137.4	2.9	194.6	47.6
YGX-6	231–2	0.02084	0.00047	0.14638	0.00748	0.05103	0.00253	132.9	3.0	138.7	6.6	242.3	110.4
	124–1	0.02130	0.00032	0.36985	0.00891	0.12591	0.00314	135.9	2.0	319.5	6.6	2041.6	43.4
	129–1	0.02109	0.00031	0.28177	0.00524	0.09688	0.00167	134.6	1.9	252.1	4.2	1564.8	31.9
	132–1	0.02088	0.00026	0.29251	0.00475	0.10159	0.00160	133.2	1.7	260.5	3.7	1653.5	28.8
	201–4	0.02124	0.00030	0.41487	0.00959	0.14166	0.00337	135.5	1.9	352.4	6.9	2247.5	40.6
	216–2	0.02103	0.00025	0.42338	0.00562	0.14605	0.00176	134.1	1.6	358.5	4.0	2300.1	20.5
	217–2	0.02191	0.00027	0.39889	0.00543	0.13203	0.00165	139.7	1.7	340.8	3.9	2125.2	21.7
	223–1	0.02128	0.00026	0.40404	0.00607	0.13769	0.00201	135.8	1.6	344.6	4.4	2198.3	25.2
	223–2	0.02118	0.00028	0.23805	0.00386	0.08153	0.00124	135.1	1.7	216.8	3.2	1234.2	29.4
	313–2	0.02142	0.00026	0.39754	0.00597	0.13463	0.00196	136.6	1.6	339.9	4.3	2159.2	25.1
XLK-3	317–2	0.02091	0.00032	0.15916	0.00380	0.05521	0.00126	133.4	2.0	150.0	3.3	420.6	49.7

been measured with LA-ICPMS and the weighted average ages and the lower intercept ages have been calculated with the ISOPLOT program (ver. 2.06) (Ludwig, 1999) (Table 2).

U–Pb data from three samples (DP-3, YGX-6, and HK-3) are nearly concordant, yielding weighted average $^{206}Pb/^{238}U$ ages of 133.6 ± 1.0 Ma (MSWD = 0.85, n = 14) (Fig. 7a), 133.7 ± 1.3 Ma (MSWD = 0.32, n = 12) (Fig. 7b), and 132.9 ± 1.5 Ma (MSWD = 0.22, n = 8) (Fig. 7c) for the Dangping, Yaogangxian and Hukeng tungsten deposits, respectively. The other two samples (TXK-3 and TSL-3) yield discordant U–Pb ages with a collinear array. These zircons suffered the metamictization to some extent and probably had slight U loss. The lower intercepts are thus interpreted as the crystallization ages for these two samples, which are 134.4 ± 1.9 Ma (MSWD = 0.13) (Fig. 7d) and 134.2 ± 1.6 Ma (MSWD = 0.27) (Fig. 7e) for the Taoxikeng and Tieshanlong tungsten deposits, respectively.

Five U–Pb ages from different areas of the Nanling Range vary from 132.9 ± 1.5 Ma to 134.4 ± 1.9 Ma (Table 3), with a weighted mean age of 133.7 ± 1.3 Ma. These hydrothermal zircon ages should represent the tungsten mineralization time. This hypothesis is supported by the following arguments: (1) Even though no zircon was found in WQV in the Xingluokeng tungsten deposit, zircons in the associated greisen (XLK-3) have hydrothermal characteristics. The morphology and geochemistry of XLK-3 zircons are similar to the above-mentioned WQV hydrothermal zircons. U–Pb ages from XLK-3 zircons show minor discordance with a lower intercept of the best-fit regression at 133.4 ± 2.9 Ma (MSWD = 1.07) (Fig. 7f and Table 3). (2) Although most researchers (Chen et al., 2006b; Lu et al., 2006; Peng et al., 2007; Yuan et al., 2008; Wang et al., 2012b; Zeng et al., 2009; Zhang et al., 2009; Hua et al., 2010; Lei et al., 2010; Bai et al., 2013; and references therein) accept the 155 ± 5 Ma as the peak age of tungsten mineralization in the Nanling Range, some K–Ar, Ar–Ar, Rb–Sr, Sm–Nd, and Re–Os ages from tungsten ore, ranging between 130 Ma and 135 Ma, have been reported (Li et al., 1993, 2006; Mao et al., 2004; Chen et al., 2006a; Luo et al., 2006; Zeng et al., 2009; Zhang et al., 2009). These ages agree with U-Pb zircon crystallization ages of the WQV zircons from this study.

6. Puzzle about the orthomagmatic model

Molybdenite Re–Os dating is considered to be a robust method for determining the age of mineralization (Suzuki et al., 1996; Stein et al., 1997, 1998). Since 1990, this method has been used to date vein-type tungsten deposits in the Nanling Range. Re-Os ages range between 224.0 Ma (Cai et al., 2006) to 95.4 Ma (Li et al., 2008), with a peak age of 155 ± 5 Ma (Chen et al., 2006b; Lu et al., 2006; Peng et al., 2007; Mao et al., 2007; Liu et al., 2008; Zeng et al., 2009; Zhang et al., 2009; Lei et al., 2010; Wang et al., 2012b; and references therein). Other types of mineral systems, such as tin (Mao et al., 2004; Peng et al., 2007; Yuan et al., 2008), copper (Lu et al., 2006; Chen et al., 2012), molybdenum mineralization (Meng et al., 2007; Wang et al., 2012b), and lead-zinc (Lei et al., 2010), have similar 155 ± 5 Ma ages. Thus, this time has been commonly accepted as the peak period for the mineralization in this area (Mao et al., 2004; Hua, 2005; Feng et al., 2011).

Vein-type tungsten deposits in the Nanling Range spatially coexist with the early Yanshanian BM (150–160 Ma). WQVs occur either around the granitic plutons (Cai et al., 2006; Chen et al., 2006b; Xu et al., 2008; Guo et al., 2010), or crosscut them (Guo et al., 2010; Feng et al., 2011). This spatial–temporal appearance of the granitic intrusion and the tungsten mineralization has led to the concept that the WQV could be genetically related to the early Yanshanian granite (Mao et al., 2004; Mei et al., 2004; Shu et al., 2011; Xu et al., 2011; and references therein). An orthomagmatic model (Mao et al., 2007; Xi et al., 2007; Zhou et al., 2010) has been used to describe the tungsten ore in the Nanling Range: fractional crystallization of granitic magma promoted the ore-forming process (ore-metals, fluxing components, and aqueous fluid), and the ore formed along fractures during or/and after the solidification of granite (Burnham, 1979; Candela, 1997; Audétat, 2000; Pirajno, 2009). The following observations also support the orthomagmatic model: (1) $\delta^{18}O$ values of quartz and whole rock from granite are consistent with those of WQV quartz (Guo et al., 2010; Song et al., 2011; Wang et al., 2012a). (2) The coexistence of both gas–liquid and liquid-melt inclusions in the WQV quartz indicates the coexistence of silicate melt and ore-forming fluid hydrothermal fluid (Chang and Huang, 2001). (3) $\delta^{34}S$ from pyrite and arsenopyrite (Song et al., 2011; Wang et al., 2012a) and δD from fluid inclusions in quartz (Guo et al., 2010; Song et al., 2011; Zhang et al., 2012) from the WQV commonly fall in the field of magmatic fluid. All of these features could indicate magmatic origin of the ore-forming materials.

However, the orthomagmatic model is based on the ore ages of 155 ± 5 Ma. The following geological facts cannot be explained by the orthomagmatic model. (1) The early Yanshanian BM is the most abundant igneous rock in the Nanling Range (Guiyang Institute of Geochemistry, 1979; Hua, 2005; Li et al., 2007a; Mao et al., 2007; Shen et al., 2007; Shu et al., 2011). Even so, not all the BMs contain tungsten ore. Most tungsten deposits are found in the middle Nanling Range, i.e., from southern Hunan Province to western Jiangxi Province (Xu et al., 2011). (2) Tungsten deposit size is not related to the size of granitic intrusion; for example, no tungsten ore exists in the Fogang granite, which is the largest batholith (its outcrop surface >6000 km^2, after Li et al., 2007b) in the Nanling Range. The orebodies can be located within any part of the granite; for example, the Xingluokeng tungsten deposit occurs at the center of the granitic batholith, the Dajishan tungsten deposit is at the top of the batholith, and the Dangping tungsten deposit is situated along the flank of the batholith (Mei et al., 2004). (3) The

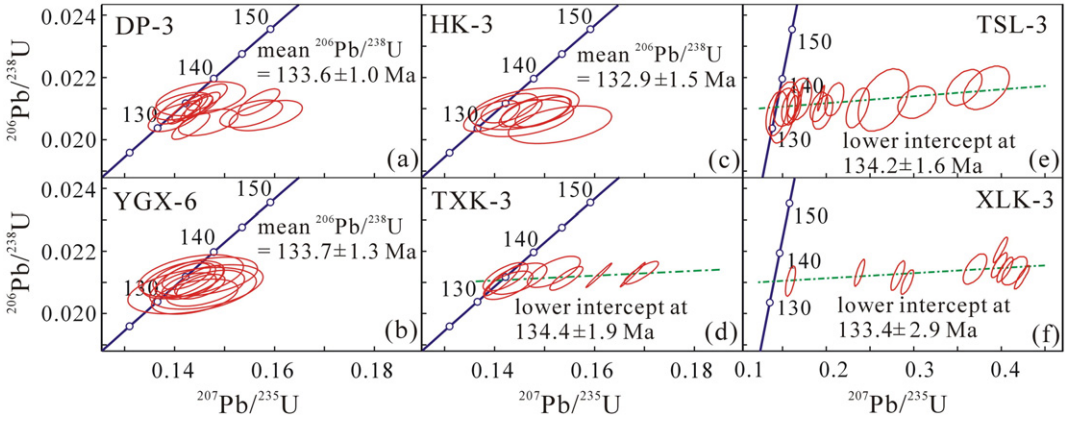

Fig. 7. U–Pb concordia diagrams of LA–ICPMS analyses for the hydrothermal zircon from WQV in the following tungsten deposits (data from Table 2): (a) Dangping (DP-3); (b) Hukeng (HK-3); (c) Yaogangxian (YGX-6); (d) Taoxikeng (TXK-3); (e) Tieshanlong (TSL-3); and (f) the hydrothermal zircons from a mineralized greisen, Xingluokeng (XLK-3).

Table 3
Summary of ages for the six studied tungsten deposits and their granitic plutons in the Nanling Range.

Deposit	Locality (province)	Biotite monzogranite			Tungsten ore		
		Age (Ma)	Method	Reference	Age (Ma)	Method	Reference
Dangping	Jiangxi	155.0–156.5	Zircon U–Pb	Yang et al., 2009	137.3	Fluorite Sm–Nd	Chen et al., 2006b
					130.0	Quartz Rb–Sr	Chen et al., 2009
					133.6	Zircon U–Pb	This study
Hukeng	Jiangxi	161.0	Zircon U–Pb	Lou et al., 2005	150.2	Molybdenite Re–Os	Liu et al., 2008
					140.3–144.1	Mica Ar–Ar	Chen et al., 2009
					132.9	Zircon U–Pb	This study
Taoxikeng	Jiangxi	157.6–158.7	Zircon U–Pb	Guo et al., 2010	154.4	Molybdenite Re–Os	Guo et al., 2010
					152.7–153.4	Muscovite Ar–Ar	Guo et al., 2010
					153.7–161.0	Quartz Rb–Sr	Guo et al., 2007
					154.4	Molybdenite Re–Os	Chen et al., 2006a,b
					155.8	Molybdenite Re–Os	Wang et al., 2012a,b
					134.4	Zircon U–Pb	This study
Tieshanlong	Jiangxi	152.4	Zircon U–Pb	Fang et al., 2012	134.2	Zircon U–Pb	This study
Yaogangxian	Hunan	155.4–157.6	Zircon U–Pb	Li et al., 2011	154.9	Molybdenite Re–Os	Peng et al., 2006
					153.0,	Mica Ar–Ar	Peng et al., 2006
					156.0–175.8	Quartz Rb–Sr	Wang et al., 2009
					170.0	Molybdenite Re–Os	Wang et al., 2009
					161.0	Molybdenite Re–Os	Wang et al., 2012a,b
					153.0–163.0	Molybdenite Re–Os	Wang, 2008
					133.7	Zircon U–Pb	This study
Xingluokeng	Fujian	155.0	Biotite K–Ar	Zhang et al., 2008	156.3	Molybdenite Re–Os	Zhang et al., 2008
					147.5	Quartz Rb–Sr	Zhang et al., 2008
					133.4	Zircon U–Pb	This study

granitic plutons are commonly crosscut by the WQV (Hua, 2005; Chen et al., 2006b) and a single WQV can extend downwards for more than one thousand meters within the Yaogangxian pluton (Tan, 1987). (4) The early Yanshanian BM in the Nanling Range is slightly peraluminous (Shen et al., 2007; Li et al., 2007a), with a high La/Lu ratio and a gentle Eu anomaly (Fig. 8), suggesting low degrees of feldspar fractionation. The low W content in this granite (5.9 ppm, Guiyang Institute of Geochemistry, 1979) is theoretically not able to accumulate enough metal (several ten thousand tons of WO_3) to form the giant or super-giant tungsten deposit via fractional crystallization. (5) Initial $^{87}Sr/^{86}Sr$ ratios of some BM in the Nanling Range vary between 0.719 and 0.741 (Liu et al., 1984), within the S-type granite range (Liu et al., 1984; Hua, 2005; Zhang et al., 2012). S-type granite batholiths commonly form in intracontinental orogenic settings during crustal thickening (de Yoreo et al., 1989; Brown, 1994). Granitoids formed during crustal thickening are not usually associated with large-scale mineral systems (Guild, 1972; Zhai, 1997). In contrast, most metal mineralization occurs in extensional settings (Groves and Bierlein, 2007; Bastos Neto et al., 2009), where large-scale fractures and faults in the upper continental crust channel ore-forming fluid and provided the space for ore deposits (Burnham, 1979; Haapala and Lukkari, 2005; Pirajno, 2009). The fact is that the early Yanshanian magmatism (in a period from 160 Ma to 150 Ma) and tungsten mineralization (at 133.7 ± 1.3 Ma) in the Nanling Range are associated with different tectonic settings. The stress field in the Nanling Range converted from compressional to extensional at ~140 Ma (Gilder et al., 1996; Li, 1999; Ren et al., 1999).

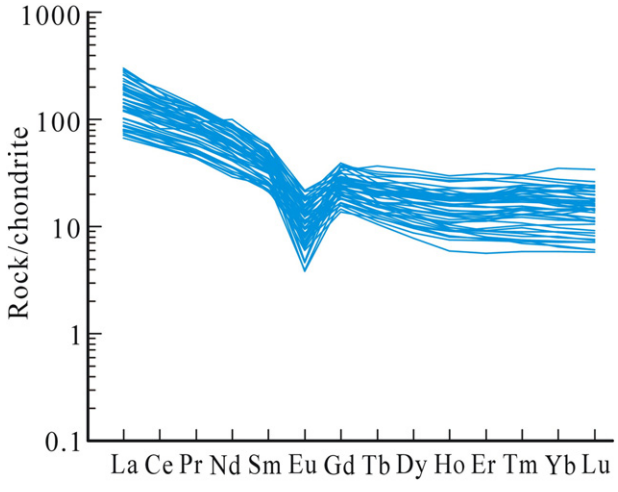

Fig. 8. Chondrite-normalized REE pattern of early Yanshanian BM in the Nanling Range. Data are from Man (1985); Huang et al. (2000); Cai et al. (2004); Mao et al. (2010); Chen et al. (2007a,b); Hua et al. (2007), Liu et al. (2007), Qiu and Hu (2007); Xu et al. (2007); Zhu et al. (2007); Wang (2008) and Wu et al. (2008).

7. Future research

Because of the 20 m.y. time difference between the BM emplacement ages (i.e., 150–160 Ma) and the ore-forming ages (i.e., 133.7 ± 1.3 Ma) (Table 3) and the geological features mentioned above, whether there is any direct relationship between the BM and the WQV is worthy of further investigation. The following observations lead us to seek a new metallogenic model for tungsten mineralization in the Nanling Range:

(1) Most molybdenite Re–Os ages from the WQV (i.e., 155 ± 5 Ma) (Chen et al., 2006b; Lu et al., 2006; Mao et al., 2007; Peng et al., 2007; Liu et al., 2008; Zeng et al., 2009; Zhang et al., 2009; Lei et al., 2010; Wang et al., 2012b; and references therein) are similar to the emplacement ages of BM (150–160 Ma) and Re/Os ratios are similar between WQV and BM (Hua, 2005; Li et al., 2007a; Shen et al., 2007; Mao et al., 2007; Zhang et al., 2008; Yang et al., 2009; Li et al., 2011; Shu et al., 2011; Fang et al., 2012; and references therein). Additionally, many studies of stable isotopes (O, S, H, etc.) show the similar compositions between WQV and the BM (Chang and Huang, 2001; Guo et al., 2010; Song et al., 2011; Wang et al., 2012a; Zhang et al., 2012). These features further indicate that the Re–Os isotopes in the WQV might be directly inherited from the BM. Therefore, the Re–Os ages reflect the BM magma age rather mineralization age.

(2) Even though most ore ages are around 155 ± 5 Ma (Chen et al., 2006b; Lu et al., 2006; Mao et al., 2007; Peng et al., 2007; Liu et al., 2008; Yuan et al., 2008; Wang et al., 2012b; Zeng et al., 2009; Zhang et al., 2009; Hua et al., 2010; Lei et al., 2010; Bai et al., 2013; and references therein), it is also noticeable that some range between 155 ± 5 Ma and 130 Ma (Chen et al., 2006a). This further suggests that even there

is a tectonic–magmatic-hydrothermal evolution potential between the BM and the WQV, the BM is not the direct source for WQV.

(3) Tungsten deposits are spatially associated with BM plutons in the Nanling Range (Cai et al., 2006; Chen et al., 2006b; Xu et al., 2008; Guo et al., 2010; Feng et al., 2011). From a tectonic point of view, BM emplacement in the Nanling Range was generally controlled by large-scale faults, which have been considered to be the same paths for the WQV emplacement (Chen et al., 2005; Zeng, 2006).

The above-mentioned phenomena lead us to seek a new metallogenic model for the tungsten mineralization in the Nanling Range. The BM could be considered as one metallogenic indicator for these tungsten deposits. Other necessary conditions should exist for the formation of the WQV during the tectonic-magmatic-hydrothermal evolution of the BM. In fact, there are many late stages of intrusive rocks. They occur generally as laccolith or stock, such as muscovite granite, alaskite, granitic porphyry, quartz porphyry, pegmatite, aplite, etc., either around or within Nanling Range BM plutons. Future metallogenic research should target such later-stage minor magmatic bodies.

8. Conclusions

WQV zircons crystallized at the same time as wolframite from the late stage or subsolidus magmatic-hydrothermal fluids. They are chemically and crystallographically similar to the zircons crystallized from the volatile-rich granitic pegmatites and distinctly different from the zircons crystallized from granitic magma. They have the following characteristics: (1) pale brown, murky brown or orange-red in color, and translucent under the microscope; (2) {110} + {101} type crystallographic form; (3) weak CL signal; (4) enrichment of Hf (ranging from 1.97 to 7.83 wt.% HfO_2), U (ranging from 0.02 to 3.97 wt.% UO_2), Th (ranging from 0 to 0.65 wt.% ThO_2), and P (ranging from 0 to 1.82 wt.% P_2O_5); and (5) presence of solid (hydrothermal and ore minerals) and fluid inclusions. These features indicate that WQV zircons are of hydrothermal origin, i.e., they were formed during the tungsten mineralization process. Therefore, the crystallization ages of hydrothermal zircons should represent the time of tungsten mineralization in the Nanling Range.

Three weighted averages of zircon $^{206}Pb/^{238}U$ ages and two lower intercept ages, ranging from 134.4 ± 1.9 Ma to 132.9 ± 1.5 Ma, with a weighted mean age of 133.7 ± 1.3 Ma, are reported in this study. The samples are from five tungsten deposits located in three provinces. The nearly identical ages of those samples indicate that the vein-type tungsten deposits were formed almost at the same time.

The tomographic and chemical characteristics of the WQV zircons indicate that the zircons formed from the same hydrothermal system as the ore mineral wolframite. The crystallization age of WQV zircons should be the same as the age of tungsten mineralization in the Nanling Range. Nanling Range tungsten mineralization may not have direct correlation with the early Yanshanian BM (150–160 Ma). Future mineral exploration in the Nanling Range should aim to reconstruct the regional geological processes which induced hydrothermal activity.

Acknowledgments

This study is supported by the National Natural Science Foundation of China (Project Nos. 41372065 and 40972058). We thank Huang, P.Y. and Wu, B. for their assistance with field trip and laboratory work. We thank an anonymous reviewer for his insightful comments for the first submission of this manuscript and Robert J. Stern, Dan Miggins, and Gina Sully for their editorial review of this current version.

References

Audétat, A., 2000. Causes for large-scale metal zonation around mineralized plutons: fluid inclusion LA–ICP-MS evidence from the mole granite, Australia. Econ. Geol. 95, 1563–1581.

Audétat, A., Pettke, T., Heinrich, C.A., Bodnar, R.J., 2008. The composition of magmatic-hydrothermal fluids in barren and mineralized intrusions. Econ. Geol. 103, 877–908.

Badanina, E.V., Trumbull, R.B., Dulski, P., Wiedenbeck, M., Veksler, I.V., Syritso, L.F., 2006. The behavior of rare-earth and lithosphile trace elements in rare-metal granites: a study of fluorite, melt inclusions and host rocks from the Khangilay complex, Transbaikalia, Russia. Can. Mineral. 44, 667–692.

Bai, X.J., Wang, M., Jiang, Y.D., Qiu, H.N., 2013. Direct dating of tin-tungsten mineralization of the Piaotang tungsten deposit, South China, by $^{40}Ar/^{39}Ar$ progressive crushing. Geochim. Cosmochim. Acta 114, 1–12.

Bastos Neto, A.C., Pereira, V.P., Ronchi, L.H., de Lima, E.F., Frantz, J.C., 2009. The world-class Sn, Nb, Ta, F (Y, REE, Li) deposit and the massive cryolite associated with the albite-enriched facies of the Madeira A-type granite, Pitinga mining district, Amazonas state, Brazil. Can. Mineral. 47, 1329–1357.

Black, L.P., Gulson, B.L., 1978. The age of the Mud Tank carbonatite, Strangways Range, Northern Territory. BMR J. Aust. Geol. Geophys. 3, 227–232.

Blanc, P., Arbey, F., Cros, P., Cesbron, F., Ohnenstetter, D., 1994. Applications de la microscopie electronique à balayage et de la cathodoluminescence à des materiaux géologiques (sulfates, carbonates, silicates). Bull. Soc. Géol. Fr. 165, 341–352.

Brown, M., 1994. The generation, segregation, ascent and emplacement of granite magma: the migmatite-to-crustally-derived granite connection in thickened orogens. Earth Sci. Rev. 36, 83–130.

Burnham, C.W., 1979. Magmas and hydrothermal fluids. In: Barnes, H.L. (Ed.), Geochemistry of Hydrothermal ore Deposits. John Wiley and Sons, New York, pp. 71–136.

Cai, J.H., Wei, C.S., Mao, X.D., Chen, K.X., Cai, M.H., 2004. Characters of mineralizing geology and metallogenic pattern of Furong tin orefield in southern Hunan Province. Geol. Sci. Technol. Inf. 23, 69–76 (in Chinese with English abstract).

Cai, M.H., Chen, K.X., Qu, W.J., Liu, G.Q., Fu, J.M., Yin, J.P., 2006. Geological characteristics and Re–Os dating of molybdenites in Hehuaping tin-polymetallic deposit, southern Hunan province. Mineral Deposits 25, 263–268 (in Chinese with English abstract).

Caironi, V., Colombo, A., Tunesi, A., Gritti, C., 2000. Chemical variations of zircon compared with morphological evolution during magmatic crystallization: an example from the Valle del Cervo Pluton (Western Alps). Eur. J. Mineral. 12, 779–794.

Candela, P.A., 1997. A review of shallow, ore-related granites: textures, volatiles and ore metals. J. Petrol. 38, 1619–1633.

Cassedanne, J.P., Baptista, A., Černý, P., 1985. Zircon hafnifère, samarskite et columbite d'une pegmatite du Riodoce, Minas Gerais, Bresil. Can. Mineral. 23, 563–567.

Černý, P., Slivola, J., 1980. The Tanco pegmatite at Berbic Lake, Manitoba. XII. Hafnian zircon. Can. Mineral. 18, 313–321.

Chang, H.L., Huang, H.L., 2001. Discovery and its significance of melt inclusions within beryl from the wolframite-quartz veins in Xihuashan Orefield, Jiangxi. Geol. Miner. Resour. South China 17, 21–27 (in Chinese with English abstract).

Chen, Q., Xu, H.C., He, Z.H., Huang, G.F., 2005. Ore-controlling features of Qianlishan–Dayishan–Jiuyishan triangle mineralization region, Hunan province. Geol. Miner. Resour. South China 21 (1), 31–46 (in Chinese with English abstract).

Chen, Y.C., Li, X.H., Li, H.Q., Chen, J.F., Xue, C.J., 2006a. Precise dating of large-scale mineralization and ore-forming pedigree. In: Mao, J.W., Hu, R.Z., Chen, Y.C., Wang, Y.T. (Eds.), Large-Scale ore-Forming Events and Large ore Dense Areas. Geological Publishing House, Beijing, pp. 58–116 (in Chinese).

Chen, Z.H., Wang, D.H., Qu, W.J., Chen, Y.C., Wang, P.A., Xu, J.X., Zhang, J.J., Xu, M.L., 2006b. Geological characteristics and mineralization age of the Taoxikeng tungsten deposit in Chongyi County, southern Jiangxi province, China. Geol. Bull. China 25, 496–501 (in Chinese with English abstract).

Chen, P.R., Zhang, M., Chen, W.F., 2007a. The Dadongshan granitic pluton. In: Zhou, X.M. (editor in chief), Granite Petrogenesis and Lithospheric Dynamics of Late Mesozoic in Nanling Range, Beijing, Science Press, 382–394 (in Chinese).

Chen, P.R., Zhang, M., Chen, W.F., 2007b. The Jiufeng–Zhuguangshan granitic pluton. In: Zhou, X.M. (editor in chief), Granite Petrogenesis and Lithospheric Dynamics of Late Mesozoic in Nanling Range, Beijing, Science Press, 533–549 (in Chinese).

Chen, M.H., Zhang, W., Xiang, J.F., Yang, Z.X., Ye, H.S., 2009. Characteristics of the ore bearing ductile shear zones at Hukeng tungsten deposit and ^{40}Ar-^{39}Ar geochronological constraints. Journal of Guilin University of Technology 29, 195–206 (in Chinese with English abstract).

Chen, F.W., Li, H.Q., Wang, D.H., Xiao, G.M., Yang, X.J., Gao, Y.W., Mei, Y.P., Lin, X.G., 2012. Geological characteristics and diagenetic–metallogenic chronological study of the Yuanzhuding porphyry Cu–Mo deposit, western Guangdong province. Acta Geol. Sin. 86, 1298–1305 (in Chinese with English abstract).

Claiborne, L.L., Miller, C.F., Walker, B.A., Wooden, J.L., Mazdab, F.K., Bea, F., 2006. Tracking magmatic processes through Zr/Hf ratios in rocks and Hf and Ti zoning in zircons: an example from the Spirit Mountain batholith, Nevada. Mineral. Mag. 70, 517–543.

Claoué-Long, J.C., King, R.W., Kerrich, R., 1990. Archean hydrothermal zircon in the Abitibi greenstone belt: constraints on the timing of gold mineralization. Earth Planet. Sci. Lett. 98, 109–128.

Correia Neves, J.M., Nunes, J.E.L., 1974. High hafnium members of the zircon-hafnon series from the granite pegmatites of Zambéria, Mozambique. Contrib. Mineral. Petrol. 48, 73–84.

Crowley, J.L., Brown, R.L., Gervais, F., Gibson, H.D., 2008. Assessing inheritance of zircon and monazite in granitic rocks from the Monashee complex, Canadian Cordillera. Journal of Petrology. J. Petrol. 49, 1915–1929.

Cuney, M., 1980. Preliminary results on the petrology and fluid inclusions of the Rössing uraniferous alaskites. Geol. Soc. S. Afr. Trans. Proc. 83, 39–45.

Davis, G.L., Hart, S.R., Tilton, G.R., 1968. Some effects of contact metamorphism on zircon ages. Earth Planet. Sci. Lett. 5, 27–34.

de Yoreo, J.J., Lux, D.R., Guidotti, C.V., 1989. The Role of Crustal Anatexis and Magma Migration in Regions of Thickened Continental Crust. In: Daly, J.G., Cliff, R.A., Yardley,

B.W.D. (Eds.), Evolution of Metamorphic Belts, Geological Society of London, Special Publications 43, pp. 187–202.
DePaolo, D.J., 1988. Age dependence of the composition of continental crust as determined from Nd isotopic variations in igneous rocks. Earth Planet. Sci. Lett. 59, 263–271.
Dickin, A.P., 1995. Radiogenic Isotope Geology. Cambridge University Press, Cambridge (490 pp.).
Dodson, M.H., McCleland-Brown, E., 1985. Isotopic and palaeomagnetic evidence for rates of cooling, uplift and erosion. Geol. Soc. Lond. Mem. 10, 315–325.
Dubinska, E., Bylina, P., Kozlowski, A., Dorr, W., Nejbert, K., Schastok, J., Kulicki, C., 2004. U–Pb dating of serpentinization: hydrothermal zircon from a metasomatic rodingite shell (Sudetic ophiolite, SW Poland). Chem. Geol. 203, 183–203.
Erlank, A.J., Smith, H.S., Marchant, J.W., Cardoso, M.P., Ahrens, L.H., 1978. Hafnium. In: Wedepohl, K.H. (Ed.), Handbook of Geochemistry. Springer-Verlag, Berlin, Heidelberg, New York.
Ewing, R.C., Meldrum, A., Wang, L.M., Weber, W.J., Corrales, L.R., 2003. Radiation effects in zircon. Rev. Mineral. Geochem. 53, 387–425.
Fang, G.C., Chen, Y.C., Chen, Z.H., Chen, Z.Y., Zhao, Z., Huang, F., 2012. Characteristics and age of zircons of Bai'e granite in South Jiangxi and its enlightment of multistage mineralization. Rock Min. Anal. 31 (3), 559–566 (in Chinese with English abstract).
Feng, C.Y., Huang, F., Zeng, Z.L., Qu, W.J., Ding, M., 2011. Isotopic chronology of Jiulongshan granite and Hongshuizhai greisens-type tungsten deposit in South Jiangxi province. J. Jilin Univ. (Earth Sci. Ed.) 41, 111–121 (in Chinese with English abstract).
Fu, B., Mernagh, T.P., Kita, N.T., Kemp, A.I.S., Valley, J.W., 2009. Distinguishing magmatic zircon from hydrothermal zircon: a case study from the Gidginbung high-sulphidation Au–Ag–(Cu) deposit, SE Australia. Chem. Geol. 259, 131–142.
Gbelsky, J., 1979. Electron microprobe determination of Zr/Hf ratios in zircons from pegmatites of the male Karpaty Mts (West Carpathians). Geol. Carpath. 30, 463–474.
Gilder, S.A., Gill, J., Coe, R.S., Zhao, X.X., Liu, Z.W., Wang, G.X., Yuan, K.R., Liu, W.L., Kuang, G.D., Wu, H.R., 1996. Isotopic and paleomagnetic constrains on the Mesozoic tectonic evolution of South China. J. Geophys. Res. Solid Earth Sect. 101 (B7), 16137–16154.
Grieco, G., Ferrario, A., von Quadt, A., Koeppel, V., Mathez, E.A., 2001. The zircon-bearing chromitites of the phlogopite peridotite of Finero (Ivrea Zone, Southern Alps): evidence and geochronology of a metasomatized mantle slab. J. Petrol. 42, 89–101.
Griffin, W.L., Powell, W.J., Pearson, N.J., O'Reilly, S.Y., 2008. GLITTER: data reduction software for laser ablation ICP-MS. In: Sylvester, P. (Ed.)Laser Ablation-ICP-MS in the Earth Sciences: Mineralogical Association of Canada Short Course Series 40, pp. 204–207 (Appendix 2).
Groves, D.I., Bierlein, F.P., 2007. Geodynamic settings of mineral deposit systems. J. Geol. Soc. 164, 19–30.
Guild, P.M., 1972. Metallogeny and the new Global Tectonics. Proceedings of the 24th IGC, Montreal 4, pp. 17–24.
Guiyang Institute of Geochemistry (Chinese Academy of Sciences), 1979n. Geochemistry of Granitoids in South China. Science Press, Beijing, pp. 1–421 (in Chinese).
Guo, C.L., Wang, D.H., Chen, Y.C., Wang, Y.B., Chen, Z.H., Liu, S.B., 2007. Precise zircon SHRIMP U-Pb and quartz vein Rb-Sr dating of Mesozoic Taoxikeng tungsten polymetallic deposit in Southern Jiangxi. Miner. Depos. 26, 432–442 (in Chinese with English abstract).
Guo, W.G., Jiang, J.Z., Gan, X.P., 2010. Research on the ore deposit geologic characteristics and metallogenic model of Yaogangxian tungsten deposit, Hunan Province. Miner. Resour. Geol. 24, 308–313 (in Chinese with English abstract).
Haapala, I., Lukkari, S., 2005. Petrological and geochemical evolution of the Kymi stock, a topaz granite cupola within the Wiborg rapakivi batholith, Finland. Lithos 80, 347–362.
Harris, A.C., Kamenetsky, V.S., White, N.C., Steele, D.A., 2004. Volatile phase separation in silicic magmas at Bajo de la Alumbrera porphyry Cu–Au deposit, NW Argentina. Resour. Geol. 54, 341–356.
Heaman, L.M., Parrish, R., 1991. U–Pb geochronology of accessory minerals. In: Heaman, L.M., Ludden, J.N. (Eds.), Applications of radiogenetic isotope systems to problems in geology, Mineralogical Association of Canada, Toronto, Short Course Handbook 19, pp. 59–102.
Hetherington, C.J., Jercinovic, M.J., Williams, M.L., Mahan, K., 2008. Understanding geologic processes with xenotime: composition, chronology, and a protocol for electron probe microanalysis. Chem. Geol. 254, 133–147.
Hoskin, P.W.O., 2005. Trace-element composition of hydrothermal zircon and the alteration of Hadean zircon from the Jack Hills, Australia. Geochim. Cosmochim. Acta 69, 637–648.
Hua, R.M., 2005. Differences between rock-forming and related ore-forming times for the Mesozoic granitoids of crust remelting types in the Nanling Range, South China, and its geological significance. Geol. Rev. 51, 633–639 (in Chinese with English abstract).
Hua, R.M., Zhang, W.L., Yao, J.M., Chen, P.R., 2007. The Dajishan–Piaotang–Huangshaping granitic pluton. In: Zhou, X.M. (editor in chief), Granite Petrogenesis and Lithospheric Dynamics of Late Mesozoic in Nanling Range, Beijing, Science Press, 436–470 (in Chinese).
Hua, R.M., Li, G.L., Zhang, W.L., Hu, D.Q., Chen, P.R., Chen, W.F., Wang, X.D., 2010. A tentative discussion on differences between large-scale tungsten and tin mineralization in South China. Mineral Deposits 29, 9–23 (in Chinese with English abstract).
Huang, Y.Y., Chen, S.Q., Zhuang, W.M., 2000. Geological and geochemical characteristics and ages of the Lapu batholith of Guangdong. Guangdong Geology 15, 20–25 (in Chinese with English abstract).
Ireland, T.R., Williams, I.S., 2003. Considerations in zircon geochronology by SIMS. Rev. Mineral. Geochem. 53 (53), 215–241.
Jackson, S.E., Pearson, N.J., Griffin, W.L., Belousova, E.A., 2004. The application of laser ablation-inductively coupled plasma-mass spectrometry to in situ U–Pb zircon geochronology. Chem. Geol. 211, 47–69.
Kerrich, R., King, R., 1993. Hydrothermal zircon and baddeleyite in Val d'Or Archean mesothermal gold deposits; characteristics, compositions, and fluid-inclusion properties, with implications for timing of primary gold mineralization. Can. J. Earth Sci. 30, 2334–2351.
Lei, Z.H., Chen, F.W., Chen, Z.H., Xu, Y.M., Gong, S.Q., Li, H.Q., Mei, Y.P., Qu, W.J., Wang, D.H., 2010. Petrogenetic and metallogenic age determination of the Huangshaping lead-zinc polymetallic deposit and its geological significance. Acta Geosci. Sin. 31, 532–540 (in Chinese with English abstract).
Li, X.H., 1999. Cretaceous magmatism and lithosphere extension in South China: the geochronology and geochemistry constraints. In: Institute of Geochemistry Chinese Academy of Science (Ed.), Resource Environment and Sustaining Development. Science Press, Beijing, pp. 264–273 (in Chinese).
Li, H.Q., Liu, J.Q., Wei, L., 1993. Research and its Implication of Fluid Inclusions Chronology of Hypothermal Deposit. Geological Publishing House, Beijing, pp. 1–75 (in Chinese with English abstract).
Li, H.Q., Lu, Y.F., Wang, D.H., Chen, Y.C., Yang, H.M., Guo, J., Xie, C.F., Mei, Y.P., Ma, L.Y., 2006. Dating of the rock-forming and ore-forming ages and their geological significances in the Furong Orefield, Qitian Mountain, Hunan. Geol. Rev. 52, 113–121 (in Chinese with English abstract).
Li, X.H., Li, Z.X., Li, W.X., Liu, Y., Yuan, C., Wei, G.J., Qi, C.S., 2007a. U–Pb zircon, geochemical and Sr–Nd–Hf isotopic constraints on age and origin of Jurassic I- and A-type granites from central Guangdong, SE China: a major igneous event in response to foundering of a subducted flat-slab? Lithos 96, 186–204.
Li, X.H., Li, W.X., Li, Z.X., 2007b. On the genetic classification and tectonic implications of the early Yanshanian granitoids in the Nanling Range, South China. Chin. Sci. Bull. 52, 1873–1885.
Li, S.R., Wang, D.H., Liang, T., Qu, W.J., Ying, L.J., 2008. Metallogenic epochs of the Damingshan tungsten deposit in Guangxi and its prospecting potential. Acta Geol. Sin. 82, 873–879 (in Chinese with English abstract).
Li, S.T., Wang, J.B., Zhu, X.Y., Wang, Y.L., Han, Y., Guo, N.N., 2011. Chronological characteristics of the Yaogangxian composite pluton in Hunan province. Geol. Prospect. 47, 143–150 (in Chinese with English abstract).
Linnen, R.L., Keppler, H., 2002. Melt composition control of Zr/Hf fractionation in magmatic processes. Geochim. Cosmochim. Acta 66, 3293–3301.
Liu, Y.J., Zhang, J.R., Sun, C.Y., Ma, D.S., Qiao, E.G., Chen, J., 1984. The geochemical characteristics of trace elements in the granitic rocks of Southern China. In: Xu, K.Q., Tu, G.Z. (Eds.), Geology of Granites and Their Metallogenetic Relations. Jiangsu Science and Technology Press, Nanjing, pp. 511–525 (in Chinese).
Liu, C.S., Chen, X.M., Wang, R.C., Hu, H., Zhang, A.C., 2007. The Nankunshan–Lapu granitic pluton. In: Zhou, X.M. (editor in chief), Granite Petrogenesis and Lithospheric Dynamics of Late Mesozoic in Nanling Range, Beijing, Science Press, 255–294 (in Chinese).
Liu, J., Ye, H.S., Xie, G.Q., Yang, G.Q., Zhang, W., 2008. Re–Os dating of molybdenite from the Hukeng tungsten deposit in the Wugongshan area, Jiangxi Province, and its geological implications. Acta Geol. Sin. 82, 1572–1579 (in Chinese with English abstract).
London, D., 1992. The application of experimental petrology to the genesis and crystallization of granitic pegmatites. Can. Mineral. 30 (3), 499–519-540.
Lu, S.N., Li, H.K., Li, H.M., 1999. Research on isotopic geochronology of mineralization events. Earth Sci. Front. 6 (2), 335–342 (in Chinese with English abstract).
Lu, Y.F., Ma, L.Y., Qu, W.J., Mei, Y.P., Chen, X.Q., 2006. U–Pb and Re–Os isotope geochronology of Baoshan Cu–Mo polymetallic ore deposit in Hunan Province. Acta Petrol. Sin. 22, 2483–2492 (in Chinese with English abstract).
Ludwig, K.R., 1999. User's manual for isoplot/Ex version 2.06: a geochronological toolkit for microsoft excel, vol. 1a. Geochronology Center, Berkeley, pp. 1–49 (Special Publication).
Lumpkin, G.R., 1998. Rare-element mineralogy and internal evolution of the Rutherford #2 Pegmatite, Amelia County, Virginia: a classic locality revisited. Can. Mineral. 36, 339–353.
Lou, F.S., Shen, W.Z., Wang, D.Z., Shu, L.S., Wu, F.R., Zhang, R.F., Yu, J.H., 2005. Zircon U-Pb istopic chronology of the Wugongshan Dome compound granite in Jiangxi Province. Acta Geol. Sin. 79, 636–644 (in Chinese with English abstract).
Luo, H.M., Xiao, G.M., Tang, K., 2006. Characteristics of tungsten polymetal belt and ore prospecting orientation in Chengkou–Jiulian area, northern Guangdong Province. Resour. Surv. Environ. 27, 127–135 (in Chinese with English abstract).
Man, F.S., 1985. The REE patterns and origin of tungsten-related granitic rocks in South China. Mineral Deposits 4, 47–52 (in Chinese with English abstract).
Mao, J.W., Xie, G.Q., Li, X.F., Zhang, C.Q., Mei, Y.X., 2004. Mesozoic large scale mineralization and multiple lithospheric extensions from South China. Earth Sci. Front. 11, 45–55 (in Chinese with English abstract).
Mao, J.W., Xie, G.Q., Guo, C.L., Chen, Y.C., 2007. Large-scale tungsten–tin mineralization in the Nanling region, South China: metallogenic ages and corresponding geodynamic processes. Acta Petrol. Sin. 23, 2329–2338 (in Chinese with English abstract).
Mao, J.R., Li, Z.L., Zhao, X.L., Zhou, J., Ye, H.M., Zeng, Q.T., 2010. Geochemical characteristics, cooling history and mineralization significance of Zhangtiantang pluton in South Jiangxi Province, P.R. China. Chin. J. Geochem. 29, 53–64.
Masau, M., Černý, P., Cooper, M.A., Chapman, R., 2002. Monazite-(Sm), a new member of the monazite group from the Annie Claim #3 granitic pegmatite, southeastern Manitoba. Can. Mineral. 40, 1649–1655.
Mei, Y.X., Pei, R.F., Li, J.W., Fu, X.J., 2004. Metallogenic series types of Mesozoic mineral deposits in China and their evolution. Mineral Deposits 23, 190–197 (in Chinese with English abstract).
Meng, X.J., Hou, Z.Q., Dong, G.Y., Liu, J.G., Qu, W.J., Yang, Z.S., Zou, L.Y., Wan, L.J., Xiao, M.Z., 2007. The geological characteristics and Re–Os isotope age of molybdenite of the Xiongjiashan molybdenum deposit, Jiangxi Province. Acta Geol. Sin. 81, 946–951 (in Chinese with English abstract).
Mezger, K., Krogstad, E.J., 1997. Interpretation of discordance U–Pb zircon ages: an evaluation. J. Metamorph. Geol. 15, 127–140.

Minor, D.R., Mukasa, S.B., 1997. Zircon U-Pb and hornblende ^{40}Ar–^{39}Ar ages for the Dufek layered mafic intrusion, Antarctica: implications for the age of the Ferrar large igneous province. Geochim. Cosmochim. Acta 61, 2497–2504.
Nasdala, L., Wenzel, T., Pidgeon, R.T., Kronz, A., 1999. Internal structures and dating of complex zircons from Meissen Massif monzonites, Saxony. Chem. Geol. 156, 331–341.
Nasdala, L., Zhang, M., Kempe, U., Panczer, G., Gaft, M., Andrut, M., Plötze, M., 2003. Spectroscopic methods applied to zircon. Rev. Mineral. Geochem. 53, 247–267.
Partington, G.A., McNaughton, N.J., Williams, I.S., 1995. A review of the geology, mineralization, and geochronology of the Greenbushes Pegmatite, Western Australia. Econ. Geol. 90, 616–635.
Pelleter, E., Cheilletz, A., Gasquet, D., Mouttaqi, A., Annich, M., El Hakour, A., Deloule, E., Féraud, G., 2007. Hydrothermal zircons: a tool for ion microprobe U–Pb dating of gold mineralization (Tamlalt–Menhouhou gold deposit, Morocco). Chem. Geol. 245, 135–161.
Peng, J.T., Zhou, M.F., Hu, R.Z., Shen, N.P., Yuan, S.D., Bi, X.W., Du, A.D., Qu, W.J., 2006. Precise molybdenite Re-Os and mica Ar-Ar dating of the Mesozoic Yaogangxian tungsten deposit, central Nanling district, South China. Miner. Depos. 41, 661–669.
Peng, J.T., Hu, R.Z., Bi, X.W., Dai, T.M., Li, Z.L., Li, X.M., Shuang, Y., Yuan, S.D., Liu, S.R., 2007. $^{40}Ar/^{39}Ar$ isotopic dating of tin mineralization in Furong deposit of Hunan province and its geological significance. Mineral Deposits 26, 237–248 (in Chinese with English abstract).
Pirajno, F., 2009. Hydrothermal Processes and Mineral Systems. Springer (1250 pp.).
Pupin, J.P., 1980. Zircon and granite petrology. Contrib. Mineral. Petrol. 73, 207–220.
Qiu, J.S., Hu, J., 2007. The Longwo–Baishigang granitic pluton. In: Zhou, X.M. (editor in chief), Granite Petrogenesis and Lithospheric Dynamics of Late Mesozoic in Nanling Range, Beijing, Science Press, 325–365 (in Chinese).
Ren, J.S., Wang, Z.X., Chen, B.W., Jiang, C.F., Niu, B.G., Li, J.R., Xie, G.L., He, Z.J., Liu, Z.G., 1999. The Tectonics of China from a Global View: A Guide to the Tectonic map of China and Adjacent Regions. Geological Publishing House, Beijing, pp. 1–25 (in Chinese).
Rubin, J.N., Henry, C.D., Price, J.G., 1989. Hydrothermal zircon at zircon overgrowths, Sierra Blanca Peaks, Texas. Am. Mineral. 74, 865–869.
Rubin, J.N., Henry, C.D., Price, J.G., 1993. The mobility of zirconium and other "immobile" elements during hydrothermal alteration. Chem. Geol. 110, 29–47.
Schaltegger, U., Pettke, T., Audétat, A., Reusser, E., Heinrich, C.A., 2005. Magmatic-to-hydrothermal crystallization in the W–Sn mineralized Mole granite (NSW, Australia) part I: crystallization of zircon and REE-phosphates over three million years: a geochemical and U–Pb geochronological study. Chem. Geol. 220, 215–235.
Seidler, J.K., Lentz, D.R., Hall, D.C., Susak, N., 2005. Zircon-rich Ta–Nb-REE mineralization in the radioactive McKeel Lake pegmatite-aplite system, Welsford Igneous Complex, southwestern New Brunswick. Explor. Min. Geol. 14, 79–94.
Shannon, R.D., 1976. Revised effective ionic radii and systematic studies of interatomic distances in halide and chalcogenides. Acta Crystallogr. A 32, 751–767.
Shedd, 2015. http://minerals.usgs.gov/minerals/pubs/commodity/tungsten/.
Shen, W.Z., Ling, H.F., Sun, T., 2007. Geochemistry of Sr and Nd isotopes of the late Mesozoic granite-volcanic rocks in South China. In: Zhou, X.M. (editor in chief), Granite Petrogenesis and Lithospheric Dynamics of Late Mesozoic in Nanling Range, Beijing, Science Press, 123–160 (in Chinese).
Shu, X.J., Wang, X.L., Sun, T., Xu, X.S., Dai, M.N., 2011. Trace elements, U–Pb ages and Hf isotopes of zircons from Mesozoic granites in the western Nanling Range, South China: implications for petrogenesis and W–Sn mineralization. Lithos 127, 468–482.
Song, S.Q., Hu, R.Z., Bi, X.W., Wei, W.F., Shi, S.H., 2011. Hydrogen, oxygen and sulfur isotope geochemical characteristics of Taoxikeng tungsten deposit in Chongyi County, southern Jiangxi Province. Mineral Deposits 30, 1–10 (in Chinese with English abstract).
Stein, H.J., Markey, R.J., Morgan, J.W., Du, A., Sun, Y., 1997. Highly precise and accurate Re–Os ages for molybdenite from the East Qinling molybdenum belt, Shanxi Province, China. Econ. Geol. 92, 827–835.
Stein, H.J., Sundblad, K., Markey, R., Morgan, J.W., Motuza, G., 1998. Re–Os ages for Archean molybdenite and pyrite, Kuittila–Kiviso, Finland and Proterozoic molybdenite, Kabeliai, Lithuania: testing the chronometer in a metamorphic and metasomatic setting. Mineral. Deposita 33, 329–345.
Suzuki, K., Shimizu, H., Masuda, A., 1996. Re–Os dating of molybdenites from ore deposits in Japan: implication for the closure temperature of the Re–Os system for molybdenite and the cooling history of molybdenum ore deposits. Geochim. Cosmochim. Acta 60, 3151–3159.
Tan, Y.J., 1987. Some geological characters of granites related to tungsten (molybdenum and tin) mineralization and their genetic significance. Mineral Resour. Geol. 1, 11–17 (in Chinese).
Taubeneck, W.H., 1957. Zircons in the metamorphic aureole of the Bald Mountain Batholith, Elkhorn Mountains, Northeastern Oregon. Bull. Geol. Soc. Am. 68, 1803–1804.
Thomas, J.B., Bodnar, R.J., Shimizu, N., Chesner, C.A., 2003. Melt inclusions in zircon. Rev. Mineral. Geochem. 53, 63–87.
Thomas, R., Forster, H.J., Rickers, K., Webster, J.D., 2005. Formation of extremely F-rich hydrous melt fractions and hydrothermal fluids during differentiation of highly evolved tin- granite magmas: a melt/fluid-inclusion study. Contrib. Mineral. Petrol. 148, 582–601.
Tomascheck, F., Kennedy, A.K., Villa, I.M., Lagos, M., Ballhaus, C., 2003. Zircons from Syros, Cyclades, Greece: recrystallization and mobilization of zircon during high-pressure metamorphism. J. Petrol. 44, 1977–2002.
Uher, P., Černý, P., 1998. Zircon in Hercynian granitic pegmatites of the western Carpathians, Slovakia. Geol. Carpath. 49, 261–270.
van Lichtervelde, M., Salvi, S., Beziat, D., Linnen, R.L., 2007. Textural features and chemical evolution in tantalum oxides: magmatic versus hydrothermal origins for Ta mineralization in the Tanco lower pegmatite, Manitoba, Canada. Econ. Geol. 102, 257–276.
Wang, Y.L., 2008. Tectonic-magma-mineralization of the W–Sn-polymetallic ore concentration area in southern Hunan Province. Unpublished Ph.D. thesis, Chinese Academy of Geological Sciences, 1–129 (in Chinese with English abstract).
Wang, R.C., Monchoux, P., Fontan, F., 1990. Chemical composition of the hafnium-rich zircon from the Beauvoir granite (the Echassieres granitic complex, France) and their relationships with cassiterite. J. Nanjing Univ. (Earth Sci.) 2, 59–68 (in Chinese with English abstract).
Wang, X., Griffin, W.L., O'Reilly, S.Y., Zhou, X.M., Xu, X.S., Jackson, S.E., Pearson, N.J., 2002. Morphology and geochemistry of zircons from late Mesozoic igneous complexes in coastal SE China: implications for petrogenesis. Mineral. Mag. 66, 235–251.
Wang, X., Griffin, W.L., Wang, Z.C., Zhou, X.M., 2003. Hf isotope composition of zircons and implication for the petrogenesis of Yajiangqiao granite, Hunan Province, China. Chin. Sci. Bull. 48, 995–998.
Wang, X., Griffin, W.L., O'Reilly, S.Y., Li, W.X., 2007. Three stages of zircon growth in magmatic rocks from the Pingtan Complex, eastern China. Acta Geol. Sinica Engl. Ed. 81, 68–80.
Wang, X., Griffin, W.L., Chen, J., 2010. Hf contents and Zr/Hf ratios in granitic zircons. Geochem. J. 44, 65–72.
Wang, X., Griffin, W.L., Chen, J., Huang, P.Y., Li, X., 2011. U and Th contents and Th/U ratios of zircon in felsic and mafic magmatic rocks: improved zircon-melt distribution coefficients. Acta Geol. Sinica Engl. Ed. 85, 164–174.
Wang, L., Hu, M.A., Qu, W.J., Chen, K.X., Long, W.G., Yang, Z., 2012a. Zircon LA–ICP-MS U–Pb and molybdenite Re–Os dating of the Dabaoshan polymetallic deposit in northern Guangdong Province and its geological implications. Geol. China 39, 29–42 (in Chinese with English abstract).
Wang, D.H., Li, H.Q., Qin, Y., Mei, Y.P., Chen, Z.H., Qu, W.J., Wang, Y.B., Cai, H., Gong, S.Q., He, X.P., 2009. Rock-forming and ore-forming ages of the Yaogangxian tungsten deposit of Hunan Province). Rock and Mineral Analysis 28, 201–208.
Wang, D.H., Qin, Y., Chen, Z.Y., Hou, K.J., 2012b. U–Pb isotopic age and a further understanding of the ore-forming mechanism in granite from the southern Jiangxi province. Rock Miner. Anal. 31, 699–704 (in Chinese with English abstract).
Webster, J.D., Rebbert, C.R., 1998. Experimental investigation of H_2O and Cl^- solubilities in F-enriched silicate liquids: implications for volatile saturation of topaz rhyolite magmas. Contrib. Mineral. Petrol. 132, 198–207.
Wu, G.Y., Hou, Z.Q., Xiao, Q.H., Wang, T., Yan, Q.R., Chen, H.M., Ma, T.Q., 2008. REE geochemistry and petrogenesis and mineralization of the Yanshanian mineralized granites in the southern Hunan polymetallic ore-concentration region. Geol. China 35, 410–420 (in Chinese with English abstract).
Xi, B.B., Zhang, D.H., Zhou, L.M., 2007. Magmatic evolutions of several granite plutons related to Sn (W) mineralization in the Nanling region, China. Geol. Bull. Chin. 26, 1591–1599 (in Chinese with English abstract).
Xu, X.S., Lu, W.M., Fan, Q.C., 2007. The Fogang granitic pluton. In: Zhou, X.M. (editor in chief), Granite Petrogenesis and Lithospheric Dynamics of Late Mesozoic in Nanling Range, Beijing, Science Press, 236–255 (in Chinese).
Xu, J.X., Zeng, Z.L., Wang, D.H., Chen, Z.H., Liu, S.B., Wang, C.H., Ying, L.J., 2008. A new type of tungsten deposit in southern Jiangxi and the new model of "five floors + basement" for prospecting. Acta Geol. Sin. 82, 880–887 (in Chinese with English abstract).
Xu, Y.M., Zhang, Y.J., Lei, Z.H., 2011. Total tungsten resource reserve prediction of middle Nanling Range. Geol. Miner. Resour. South China 27 (39–45), 39–45 (in Chinese with English abstract).
Yang, J.H., Chen, X.Y., Wang, X.D., 2009. Zircon LA–ICPMS U–Pb dating and ore-forming fluid geochemical characteristics of Dangping tungsten-bearing granites in Jiangxi province, South China. Acta Mineral. Sin. 29 (Suppl), 339–340 (in Chinese).
Yuan, S.D., Peng, J.T., Hu, R.Z., Li, H.M., Shen, N.P., Zhang, D.L., 2008. A possible U–Pb age on cassiterite from the Xianghualing Tin-polymetallic deposit (Hunan, South China). Mineral. Deposita 43, 375–382.
Zeng, Z.F., 2006. Characteristics of ore controlling structure in Da'ao mine, Hunan and its controlling function to greisen-type tungsten and tin deposit. Mineral Resour. Geol. 20 (6), 612–617 (in Chinese with English abstract).
Zeng, Z.L., Zhang, Y.Z., Zhu, X.P., Chen, Z.H., Wang, C.H., Wu, W.J., 2009. Re–Os isotopic dating of molybdenite from the Maoping tungsten–tin deposit in Chongyi county of Southern Jiangxi Province and its geological significance. Rock Miner. Anal. 28, 209–214 (in Chinese with English abstract).
Zhai, Y.S., 1997. Macroscopic Structure and Superlarge ore Deposits. Geological Publishing House, Beijing, pp. 1–180 (in Chinese with English abstract).
Zhang, A.C., Wang, R.C., Hu, H., Zhang, H., Zhu, J.C., Chen, X.M., 2004. Chemical evolution of Nb–Ta oxides and zircon from the Koktokay No. 3 granitic pegmatite, Altai, northwestern China. Mineral. Mag. 68, 739–756.
Zhang, J.J., Chen, Z.H., Wang, D.H., Chen, Z.Y., Liu, S.B., Wang, C.H., 2008. Geological characteristics and metallogenic epoch of the Xingluokeng tungsten deposit, Fujian Province. Geotecton. Metallog. 32, 92–97 (in Chinese with English abstract).
Zhang, W.L., Hua, R.M., Wang, R.C., Li, H.M., Qu, W.J., Ji, J.Q., 2009. New dating of the Piaotang granite and related tungsten mineralization in southern Jiangxi. Acta Geol. Sin. 83, 659–670 (in Chinese with English abstract).
Zhang, D.Q., Feng, C.Y., Li, D.X., Chen, Y.C., Zeng, Z.L., 2012. Fluid inclusions characteristics and ore genesis of Taoxikeng tungsten and tin deposit in Chongyi County, Jiangxi Province. J. Jilin Univ. (Earth Sci. Ed.) 42, 374–383 (in Chinese with English abstract).
Zhou, Y.Z., Gao, C.S., Hong, Y.L., Han, Z.X., Wen, L.H., 2010. Diagenesis-mineralization process and mineralization models of Xihuashan granite. China Tungsten Ind. 25, 12–16 (in Chinese with English abstract).
Zhu, J.C., Zhang, P.H., Xie, C.F., Yang, C., 2007. The Huashan–Guposhan granitic pluton. In: Zhou, X.M. (editor in chief), Granite Petrogenesis and Lithospheric Dynamics of Late Mesozoic in Nanling Range, Beijing, Science Press, 366–382 (in Chinese).